CDF note 8206

Same Side (Kaon) Tagging in Fully Reconstructed Decays

The CDF Collaboration
URL http://www-cdf.fnal.gov

(Dated: September 17, 2006)

Preliminary Results for 2006 Winter Conferences

Based on a Monte Carlo sample we developed a Same Side (Kaon) Tagging algorithm to determine the production flavor of B_s mesons. This is a crucial step in the ongoing B_s mixing analysis. This tagger is expected to provide a large increase in the effective size of the B_s sample.
Data and Monte Carlo agreement in the high statistic B^+ and B^0 sample have been evaluated. Extensive systematic studies where performed to cover all potential discrepancies between data and Monte Carlo. The final algorithm is based on kaon identification and dilution parameterization. It achieves a tagging performance of ϵD^2 of $4.0^{+0.9}_{-1.2}$ % on the $B_s \to D_s(\phi\pi)\pi$ sample.

I. INTRODUCTION

The observation of B_s^0 mixing is one of the main goals of the CDF Run II physics program. The large expected value of the Δm_s mixing parameter makes it challenging to study and measure B_s^0 oscillations. We have recently presented new results in the search for the B_s^0 oscillation frequency [1–5], improving the current world average and increasing the expectation of a possible Δm_s determination.
So far only opposite side flavor taggers have been used in the B_s^0 mixing analysis to determine the B flavor at production. Those taggers are expected to have very small dependency on the properties of the signal side. For that reason, their performance were parameterized in a large sample of partially reconstructed B decays which has been collected by the so-called $\ell + SVT$ Trigger. This trigger selects events with a lepton with a minimum transverse momentum of 4 GeV/c and a displaced track with at least 2 GeV/c transverse momentum. To compensate potential differences (e.g. in momentum) of the ℓ+SVT sample compared to our signal B_s^0 sample we adjust the tagging performance with a global scale factor using a B^+ and B^0 samples similar to the signal sample, finding scale factors close to unit [1].
The Same Side Tagger (SST) determines the flavor of the B meson at production time looking at the charge of the fragmentation tracks around the B meson itself. This method exploits the flavor charge correlations between the B meson and associated particles produced in the hadronization process (fig. 1). In the case of the B_s the leading fragmentation track is expected to contain strangeness, thus in this case the tagger is called Same Side Kaon Tagger (SSKT).

The SS(K)T is expected to have much better performance than all opposite side flavor taggers together. But there is no straightforward way to measure its dilution on data, since the tagging characteristics depend on the particular B meson. That could only be possible if B_s mixing is observed, and the dilution is fitted from the data. Thus we have for the moment to rely on our Monte Carlo to determine the SS(K)T performance. This note summarizes the tagging performance for all B mesons: B^+, B^0 and B_s, with special attention in the B_s^0 case. Main focus of this analysis is the evaluation of the data Monte Carlo agreement in the high statistics B^0 and B^+ modes and the study of the systematic uncertainties of the prediction of the tagger performance from Monte Carlo samples for the B_s data.

II. MONTE CARLO AND DATA SAMPLES

This study has been done on data samples selected by the Di-Muon and Two-Track-Trigger. Those triggers select events with two muons with a transverse momentum of at least 1.5 GeV/c or two displaced tracks with at least 2 GeV/c transverse momentum, respectively. The study has been restricted to runs in which all relevant detector components were fully functional. The sample size corresponds to an integrated luminosity of 355 pb^{-1}.

A large PYTHIA Monte Carlo [6] sample has been generated, including flavor creation, flavor excitation and gluon splitting $b\bar{b}$ production processes with a relative ratio of about 5:11:4. While the B meson on the signal side was forced in a specific decay the other side was kept unbiased. The simulated decays are listed in Table I.

$\bar{b}$-quark	b-quark
$B_u^+ \to J/\psi K^+,\ J/\psi \to \mu^+\mu^-$	$B_u^- \to J/\psi K^-,\ J/\psi \to \mu^+\mu^-$
$B_d^0 \to J/\psi K^{*0},\ J/\psi \to \mu^+\mu^-,\ K^{*0} \to K^+\pi^-$	$\bar{B}_d^0 \to J/\psi \bar{K}^{*0},\ J/\psi \to \mu^+\mu^-, \bar{K}^{*0} \to K^-\pi^+$
$B_s^0 \to J/\psi\phi,\ J/\psi \to \mu^+\mu^-,\ \phi \to K^+K^-$	$\bar{B}_s^0 \to J/\psi\phi,\ J/\psi \to \mu^+\mu^-,\ \phi \to K^+K^-$
$B_u^+ \to \bar{D}^0\pi^+,\ D^0 \to K^-\pi^+$	$B_u^- \to D^0\pi^-,\ \bar{D}^0 \to K^+\pi^-$
$B_d^0 \to D^-\pi^+,\ D^- \to K^+\pi^-\pi^-$	$\bar{B}_d^0 \to D^+\pi^-,\ D^+ \to K^-\pi^+\pi^+$
$B_s^0 \to D_s^-\pi^+,\ D_s^- \to \phi\pi^-,\ \phi \to K^+K^-$	$\bar{B}_s^0 \to D_s^+\pi^-,\ D_s^- \to \phi\pi^+,\ \phi \to K^+K^-$

TABLE I: Signal side topologies of the Monte Carlo samples.

The default PYTHIA Lund fragmentation model was used to describe the production and properties of particles formed in the fragmentation process. The energy taken away from the b string by the B meson is

described by a symmetric Lund function, it's parameterization has been taken from fits to LEP data [7].
A fraction of 20% of the B^0 and B^+ mesons were chosen to be originated from excited B^{**} decays.

The Monte Carlo sample has been generated to reproduce luminosity weighted run-by-run the detector status similar to data.
The response of the particle identifications systems (Time-Of-Flight (TOF) and energy loss (dE/dx) in the drift chamber) have been simulated according to the resolution and efficiency distributions measured on clean particle samples in data.
The (luminosity dependent) effect of multiple interactions in the event has been taken into account by embedding tracks from data into Monte Carlo events. Additionally the Monte Carlo was corrected for the trigger prescaling which is applied in data taking at high instantenous luminosities.

We will later assign systematic uncertainties to all the assumptions which enter the Monte Carlo simulation. The range of variations will be driven by measurements on data.

The selection cuts for the B candidates are summarized in Table II. Additionally we require the z position of the fitted B vertex to be in a region with full coverage of the vertex detector, namely $[-50\text{ cm}, -18.0\text{ cm}] \bigcup [-14.0\text{ cm}, +14.5\text{ cm}] \bigcup [+18.5\text{ cm}, +50\text{ cm}]$. The according yields are reported in Table III.

	$B_u^+ \to J/\psi K^+$	$B_d^0 \to J/\psi K^{*0}$	$B_s^0 \to J/\psi \phi$
$\mathcal{P}(B_{vertex})$	$>10^{-3}$	$>10^{-4}$	$>10^{-3}$
$\chi^2_{r\phi}(B)$	—	<225	<225
$p_T(B)$ [GeV/c]	>5.0	>5.0	>4.0
$p_T(K^+, K^{*0}, \phi)$ [GeV/c]	>1.0	>1.0	>1.0
$\|m_{K\pi} - m_{K^{*0}}\|$ [MeV/c^2]	—	<50	—
$\|m_{KK} - m_\phi\|$ [MeV/c^2]	—	—	<10
$L_{xy}/\sigma_{L_{xy}}(B)$	>4.5	>4.5	>3.0
$\sigma_{L_{xy}}(B)$ [μm]	<400	<400	<400

	$B_u^+ \to \bar{D}^0\pi^+$	$B_d^0 \to D^-\pi^+$	$B_s^0 \to D_s^-\pi^+$
$\chi^2_{r\phi}(B)$	<15	<15	<15
$\chi^2_{r\phi}(D)$	<15	<15	<14
$\sigma_{L_{xy}}(B)$ [μm]	—	—	<400
$\frac{L_{xy}}{\sigma}(B)$	>8	>11	>7
$\frac{L_{xy}}{\sigma}(D)$	—	—	>2
$L_{xy}(B \leftarrow D)$ [μm]	>-150	>-300	>-200
$\|d_0(B)\|$ [μm]	<80	<110	<60
$p_T(B)$ [GeV/c]	>5.5	>5.5	>5.5
$p_T(\pi_B)$ [GeV/c]	>1.0	>1.2	>1.2
$p_T(tracks)$ [GeV/c]	—	—	>0.35
$m_{K^+K^-}$ [GeV/c^2]	—	—	[1.013, 1.280]
$\Delta R(D, \pi_B)$	<2.0	<1.5	—

TABLE II: Summary of selection cuts for B candidates. $\mathcal{P}(B_{vertex})$ is the probability of fit of the decay vertex of the B candidate. L_{xy} is the decay length of the B candidate in the $r\phi$ plane of the detector; $\chi^2_{r\phi}$ is the $r\phi$ component of the χ^2 of the vertex fit of the B candidate; d_0 is the impact parameter of a track in $r\phi$ plane relative to the primary vertex; ΔR between two directions is defined as $\sqrt{\Delta\phi^2 + \Delta\eta^2}$.

III. SAME SIDE TAGGING

The idea of flavor tagging on the signal side is explained in detail in [8]. This method exploits flavor charge correlation between the B meson and associated particles produced in the hadronization process (Fig. 1).

mode	MC	data
$B_u^+ \to J/\psi K^+$	369K	5240
$B_d^0 \to J/\psi K^{*0}$	178K	2360
$B_s^0 \to J/\psi \phi$	28K	400
$B_u^+ \to D^0 \pi^+$	239K	9270
$B_d^0 \to D^- \pi^+$	142K	8040
$B_s^0 \to D_s^- \pi^+$	34K	560

TABLE III: Data and Monte Carlo yields.

E.g. a B^0 (B_s) meson is produced by pulling a $d\bar{d}$ ($s\bar{s}$) quark pair out of the vacuum. The d (s) and the $\bar{b}$ quark form a B meson and the left over $\bar{d}$ ($\bar{s}$) quark is then likely to form a pion (kaon) together with a u quark from a $u\bar{u}$ pair. This chain goes on until no energy is left over to form further particles. In this simple picture the charge of the first pion (kaon) indicates the flavor of the B meson. Additional processes like the formation of neutral particles such as a π^0's, K^*'s, K_s's or ϕ's as leading fragmentation particles or the production of B mesons through the decay of excited B states lead to more complex scenarios. The most important task of this analysis is to evaluate wether those mechanisms are described properly in the Monte Carlo. If this is confirmed for the high statistics B^+ and B^0 modes we are assured to rely on the Monte Carlo as well for the prediction of the tagging performance for the B_s.

A. Particle Identification

In case of B_s mesons, selecting kaons in the vincinity is a very good criteria to select the leading fragmentation track. To seperate kaons from other particle species, mainly pions, information provided by the time-of-flight system (TOF) and energy loss measurement in the drift chamber (dE/dx) are used. A combined kaon probability has been defined

$$\log(LH(PID)) = \log(\frac{P_{TOF}(K)P_{dE/dx}(K)}{f_p P_{TOF}(p)P_{dE/dx}(p)+f_\pi P_{TOF}(\pi)P_{dE/dx}(\pi)}),$$

where $f_p = 0.1$ and $f_\pi = 0.9$ are a priori probabilities for the background composition and P_{TOF} and $P_{dE/dx}$ refere to probability density functions which have been determined on pure particle samples.
In case either TOF or dE/dx information is not available the according corresponding probabilites are one, thus the $\log(LH(PID))$ variable reflects the a priori probability.

B. Data Monte Carlo Agreement of Basic Event Properties

Before moving on to develop tagging algorithms and to determine their performance, data Monte Carlo agreement for several tagging related quantities were examined. To test as well correlations among kinematic and PID related variables all quantities are plotted with and without a cut on the kaon probability ($\log(LH(PID)) > 1$). All plots are B mass sideband subtracted and normalized to the number of B mesons in the data. Only plots for the $D\pi$ modes are shown, the distributions for the J/Ψ modes look very similar.

- number of tagging candidates (with/without cut on $\log(LH(PID) > 1)$, Figure 3;
- p_T of tagging candidates (with/without cut on $\log(LH(PID)) > 1$), Figure 4;
- p_T^{rel} of tagging candidates (with/without cut on $\log(LH(PID)) > 1$), Figure 5;
- p_L^{rel} of tagging candidates (with/without cut on $\log(LH(PID)) > 1$), Figure 6;
- $\log(LH(dE/dx))$ for all tagging candidates, Figure 7;
- $\log(LH(TOF))$ for all tagging candidates, Figure 8;

- $\log(LH(PID))$ for all tagging candidates, Figure 9.

We observe in general good agreement. Remaining small discrepencies will be covered by the systematic variations as shown later for the most important variables.

C. Tagging Algorithms

Tracks with a reasonable quality ($\geq$ 3 Silicon ϕ hits & COT hits, $p_T \geq 450$ MeV/c), which are likely originated from the same primary interaction as the B meson ($|d_0/\sigma_{d_0}| \leq 4$ & $|\Delta z_0(track, B)| \leq 1.2$ cm) and close to the reconstructed B meson ($\Delta R(track, B) \leq 0.7$) are considered as potential tagging tracks. Additionally, tracks which are identified as electrons or muons or which are not in a detector region of good particle idenfication ($|\eta| \geq 1$) are rejected.
In case more than one track in the event pass those criteria, and the potential tagging tracks do not have the same charge, a further selection criteria has to be introduced to actually make a tagging decision.
The following two algorithms have been studied in detail:

- The tagging track with the largest relative longitudinal momentum is chosen (max p_L^{rel} algorithm).
- The tagging track with the highest kaon probability is chosen (max $\log(LH(PID))$ algorithm).

The second algorithm is clearly not the optimal one for the B^0 case. But rather than optimizing the algorithm for B^0 and B^+ we use those high statistic B modes to test the very same algorithms which are considered to show good performance for the B_s.
An algorithm based on pure kinematics and one based on particle identification has been chosen in order to test data and Monte Carlo agreement for different properties related to the fragmentation.

D. Fitting for Tagging Performance

To determine the tagging performance a combined mass, lifetime (ct) and mixing fit has been performed which is described in detail in [1]-[5]. The signal part of the Likelihood can be written as:

$$\begin{aligned}
\mathcal{L}_{signal} &= \mathcal{L}_{signal,mass}\mathcal{L}_{signal,ct}\mathcal{L}_{signal,tagging};\\
\mathcal{L}_{signal,tagging}(B_{d,s}) &= \epsilon_{signal}\frac{1 \pm D\cos(\Delta m_{d,s}t)}{2} + (1-\epsilon_{signal})\\
\mathcal{L}_{signal,tagging}(B^+) &= \epsilon_{signal}\frac{1 \pm D}{2} + (1-\epsilon_{signal})
\end{aligned}$$

D is the so-called dilution of the tagger, which is defined as $1 - 2P_{wrong}$, where P_{wrong} is the mistag probability. ϵ_{signal} is the tagging efficiency. ($\Delta m_s = 0$ for Monte Carlo).
The fit results for both algorithms in data and Monte Carlo are shown in Tables IV, V. The quoted uncertainties are statistical only. We observe decent data/Monte Carlo agreement for all decay modes in both algorithms.

Different events have different potential dilution. Figures 10-12 display the dependence of the dilution of the max p_L^{rel} algorithm on the transverse momentum of the tagging track. Two cases are studied separately. If there is only one potential tagging track or all tagging track candidates have the same charge this is called "agreeing case". The case in which actually a decision has to be taken is called "disagreeing case". We find a better tagging performance for the agreeing case compared to the disagreeing case. Higher momentum tagging tracks provide a higher dilution.
For the max $\log(LH(PID))$ algorithm the tagging performance has been studied as a function of $\log(LH(PID))$. Events are again split up in agreeing and disagreeing cases (fig. 13-15). For the B^+ we see high dilution both for more pion and more kaon like tracks. For B^0 the pions are more likely to be correlated to the production flavor, while kaons are mainly uncorrelated (D=0). This pattern is inverted for the B_s, where kaons are potential good tagging tracks and pions do not carry any information on the B production

[%]		$B_u^+ \to J/\psi K^+$	$B_d^0 \to J/\psi K^{*0}$	$B_s^0 \to J/\psi \phi$
MC	ϵ	55.2 ± 0.1	54.4 ± 0.1	49.5 ± 0.3
	$\mathcal{D}$	25.3 ± 0.2	14.9 ± 0.3	16.2 ± 0.8
data	ϵ	60.0 ± 0.7	57.3 ± 1.0	49.1 ± 2.9
	$\mathcal{D}$	22.3 ± 1.9	10.7 ± 4.6	—
[%]		$B_u^+ \to \bar{D}^0 \pi^+$	$B_d^0 \to D^- \pi^+$	$B_s^0 \to D_s^- \pi^+$
MC	ϵ	55.9 ± 0.1	56.6 ± 0.6	52.1 ± 0.3
	$\mathcal{D}$	25.7 ± 0.3	15.1 ± 0.4	19.0 ± 0.8
data	ϵ	58.4 ± 0.5	57.2 ± 0.6	49.3 ± 2.3
	$\mathcal{D}$	25.9 ± 1.4	13.3 ± 2.9	—

TABLE IV: Performance of max p_L^{rel} algorithm in data and MC.

[%]		$B_u^+ \to J/\psi K^+$	$B_d^0 \to J/\psi K^{*0}$	$B_s^0 \to J/\psi \phi$
MC	ϵ	55.1 ± 0.1	54.4 ± 0.1	49.5 ± 0.3
	$\mathcal{D}$	24.2 ± 0.3	12.7 ± 0.3	18.9 ± 0.8
data	ϵ	60.0 ± 0.7	57.3 ± 1.0	49.1 ± 2.9
	$\mathcal{D}$	21.7 ± 1.9	10.7 ± 4.6	—
[%]		$B_u^+ \to \bar{D}^0 \pi^+$	$B_d^0 \to D^- \pi^+$	$B_s^0 \to D_s^- \pi^+$
MC	ϵ	55.9 ± 0.1	56.6 ± 0.1	52.1 ± 0.3
	$\mathcal{D}$	24.5 ± 0.3	12.9 ± 0.4	21.8 ± 0.8
data	ϵ	58.4 ± 0.5	57.2 ± 0.6	49.3 ± 2.3
	$\mathcal{D}$	25.4 ± 1.4	14.2 ± 2.9	—

TABLE V: Performance of max $\log(LH(PID))$ algorithm in data and MC.

flavor. The decrease of predicted dilution at very high kaon probability values is related to the fact that both particle ID systems (dE/dx and TOF) give best kaon pion separation for low momentum tracks. Thus the high kaon probability tracks are most likely true low momentum kaons which are coming from the underlying event. But leading fragmentation tracks are more likely to have higher momenta.

To check whether the same dependencies seen in Monte Carlo exist in data each event is assigned a predicted dilution as a function of tagging track (p_T) and $\log(LH(PID))$ respectively, which have been derived from Monte Carlo. The signal Likelihood has been modified in the following way:

$$\begin{aligned} \mathcal{L}_{signal,tagging}(B_{d,s}) &= \epsilon_{signal} \frac{1 \pm S_D D_{pred} \cos(\Delta m_{d,s} t)}{2} + (1 - \epsilon_{signal}) \\ \mathcal{L}_{signal,tagging}(B^+) &= \epsilon_{signal} \frac{1 \pm S_D D_{pred}}{2} + (1 - \epsilon_{signal}) \end{aligned}$$

where D_{pred} is the predicted dilution and S_D an overall scale factor to compensate differences between the predicted dilution and the actual asymmetry in the data. This time D_{pred} is different but fixed for each event and we fit for S_D. The according values obtained by fitting the Monte Carlo have per construction to come out very close to one. Fitting for dilution scale factors in the data is an important check of the data/Monte Carlo agreement in the shape of the predicted dilution. This is a even stronger test of the fragmentation model than the fit for the average dilution.
Additionally, using predicted dilutions improve the overall tagging performance compared to average dilutions. The number comparable to the average dilution is in this case the so-called effective dilution $S_D\sqrt{< D^2 >}$. The fit results for both algorithms in data and Monte Carlo are shown in Tables VI, VII. Statistical uncertainties only are quoted. We observe again good data/Monte Carlo agreement. About 2-4% absolute in dilution can be gained by exploiting event-by-event dilution.

	[%]	$B_u^+ \to J/\psi K^+$	$B_d^0 \to J/\psi K^{*0}$	$B_s^0 \to J/\psi \phi$
MC	ϵ	55.1 ± 0.1	54.4 ± 0.1	49.5 ± 0.3
	S_D	100.3 ± 0.7	101.1 ± 1.8	99.7 ± 4.4
	$S_D\sqrt{\langle\mathcal{D}^2\rangle}$	28.5 ± 0.2	16.8 ± 0.3	18.6 ± 0.8
data	ϵ	60.0 ± 0.2	57.3 ± 1.0	49.1 ± 2.9
	S_D	91.8 ± 6.3	85.9 ± 29.1	—
	$S_D\sqrt{\langle\mathcal{D}^2\rangle}$	26.4 ± 2.1	13.6 ± 5.4	—
	[%]	$B_u^+ \to \bar{D}^0 \pi^+$	$B_d^0 \to D^- \pi^+$	$B_s^0 \to D_s^- \pi^+$
MC	ϵ	55.9 ± 0.1	56.6 ± 0.1	52.1 ± 0.3
	S_D	100.3 ± 0.9	98.0 ± 2.1	100.5 ± 3.3
	$S_D\sqrt{\langle\mathcal{D}^2\rangle}$	29.0 ± 0.3	17.2 ± 0.4	22.8 ± 0.7
data	ϵ	58.2 ± 0.5	57.1 ± 0.6	49.3 ± 2.3
	S_D	103.6 ± 4.7	110.0 ± 16.0	—
	$S_D\sqrt{\langle\mathcal{D}^2\rangle}$	30.4 ± 1.3	19.0 ± 2.5	—

TABLE VI: Performance of parameterized max p_L^{rel} algorithm in data and Monte Carlo.

	[%]	$B_u^+ \to J/\psi K^+$	$B_d^0 \to J/\psi K^{*0}$	$B_s^0 \to J/\psi \phi$
MC	ϵ	55.1 ± 0.1	54.4 ± 0.1	49.5 ± 0.3
	S_D	100.0 ± 0.7	98.0 ± 1.7	98.8 ± 3.6
	$S_D\sqrt{\langle\mathcal{D}^2\rangle}$	27.0 ± 0.2	17.9 ± 0.3	22.3 ± 0.8
data	ϵ	60.3 ± 0.2	57.3 ± 1.0	49.1 ± 2.9
	S_D	87.6 ± 6.7	78.8 ± 25.0	—
	$S_D\sqrt{\langle\mathcal{D}^2\rangle}$	23.9 ± 2.2	13.7 ± 5.5	—
	[%]	$B_u^+ \to \bar{D}^0 \pi^+$	$B_d^0 \to D^- \pi^+$	$B_s^0 \to D_s^- \pi^+$
MC	ϵ	55.9 ± 0.1	56.6 ± 0.1	52.1 ± 0.3
	S_D	100.0 ± 0.9	98.5 ± 2.1	98.8 ± 2.5
	$S_D\sqrt{\langle\mathcal{D}^2\rangle}$	27.5 ± 0.2	17.4 ± 0.4	28.5 ± 0.7
data	ϵ	58.2 ± 0.5	57.1 ± 0.6	49.3 ± 2.3
	S_D	95.1 ± 4.7	104.7 ± 14.4	—
	$S_D\sqrt{\langle\mathcal{D}^2\rangle}$	25.7 ± 1.3	17.6 ± 2.3	—

TABLE VII: Performance of parameterized max $\log(LH(PID))$ algorithm in data and Monte Carlo.

IV. SYSTEMATIC UNCERTAINTIES

All our systematic studies related to variations of underlying physics process have been performed by either reweighting or filtering out events from the original Monte Carlo sample. Systematic variations to the particle ID response in the detector or multiple interactions have been studied by resimulating that part of the original Monte Carlo events.

The following sources of systematic uncertainties have been investigated:

PID simulation & resolution
We varied TOF and dE/dx efficiency and resolution according to measurement uncertainties in the data. This compensates as well effects of higher occupancy at higher luminosity.

B^{**} rates
The fraction of B^+ and B^0 candidates originated from B^{**} decays has been chosen to be 20% according to recent LEP measurements [9]. The B^{**} fraction does not affect the predicted tagging performance of B_s. But it contributed to the uncertainty of the high statistic B^+ and B^0 modes. We will later assign an uncertainty based on the data Monte Carlo agreement in those modes to the B_s predictions. Therefore the effect of B^{**}

rates contributes indirectly to the systematic uncertainties for the B_s predictions.
We based the systematic variations on the the B^{**} rate on the largest and smallest single experiment measurements $\pm 1\sigma$ currently available both from CDF Run I and LEP measurements. While LEP measurements consistently prefer B^{**} rates around 20% [9], a CDF Run I analysis found 28$\pm$7% [10]. We varied the rate for systematic uncertainties within 16-35%.

Production Mechanisms
As default about 5:11:4 of $b\bar{b}$ pairs are produced in flavor creation, flavor excitation and gluon splitting processes in the Monte Carlo sample. The most distinguishing variable for those processes is the angular difference $\Delta\phi$ between the signal and opposite side B direction. While flavor creation and flavor excitation mainly produce the B mesons back-to-back, B mesons from gluon splitting processes point more often in the same direction. In the context of same side tagging, opposite side B daughters and fragmentation tracks are more likely to disturb the tagger for gluon splitting events than for the two other processes. By fitting Monte Carlo $\Delta\phi$ distributions of the different processes to the $\Delta\phi$ distribution in data the following range for the systematic variations have been determined: Gluon splitting fraction within [-68%,+46%], flavor excitation and creation within [-50%,+50%] relative to their nominal appearance.

Fragmentation
The default PYTHIA Lund fragmentation model in combination with a symmetric Lund function has been chosen to produce the nominal default Monte Carlo sample. Several systematic studies related to the fragmentation have been performed:

- Fragmentation Function
  From a simultaneous fit to several distributions in data and Monte Carlo which are sensitive to the B fragmentation function, such as track multiplicity, transverse momentum of the B and of the fragmentation tracks, we have determined the allowed parameter space for the parameters of the symmetric Lund function and used those for assigning according systematic uncertainties (Fig. 16).

- Particle Content Around the B Meson
  The particle species produced around the B_s meson give us some insight to the fragmentation process. A measurement of the content of stable charged particles around B mesons have been performed in a high statistic semileptonic sample [11]. While the rates of kaons, pions and protons between data and Monte Carlo agree well for B^0 and B^+, we find 20.2$\pm$1.4% of kaons in B_s data compared to 23.6 $\pm$ 0.2 in the Monte Carlo sample use for this analysis ($p_T(B)$ dependencies of particle fractions have been already taken out). As systematic variation we reduce the kaon fraction down to 19.5% (20.2%-0.475*1.4%). This can be done in several ways, first we reweighted all events with a kaon as tagging track. But different type of kaons have different tagging power. The potential best ones are so-called prompt kaons which are directly originate from the b string. As a second systematic study only those events are reweighted such that the discrepancy between the kaon rate in data and Monte Carlo is compensated. Half of this worst case scenario has been additionally assigned as systematic uncertainty.
  Additional to the stable charged particles we checked for resonances and vector particles such as ϕ, K_s and K^*. We compare our Monte Carlo sample here to the high statistic $B_s \to \ell D_s X$ sample (fig. 17). In general good agreement has been observed although the statistical precision is not good, thus no quantitative statement can be made. Therefore the content of $\phi' s$, K_s's and K^*'s in Monte Carlo has been varied separately by a factor 2 and by a factor 0.5 respectively. The largest deviations in the tagger performance obtained in those tests has been assigned as additional systematic uncertainty.

- Variation within statistics from the data:
  Fragmentation determines the formation of hadrons out of the string. Thus it essential effects the track multiplicity around the B meson, the B momentum and the momenta of the fragmentation tracks. By varying the Monte Carlo sample within the ranges allowed by the statistical uncertainties on the corresponding distributions in the data, we obtain a model independent estimate of how far the Monte Carlo can be maximal off. This study not only covers uncertainties related to the fragmentation but essential all other potential sources of systematic uncertainties, as long as they show up in a disagreement between data and Monte Carlo in any of those distributions. The data distributions and the according Monte Carlo variations are displayed in Figure 18.

[%]	$B^+ \to J/\psi K^+$	$B^0 \to J/\psi K^*$	$B_s \to J/\psi\phi$	$B^+ \to D\pi$	$B^0 \to D\pi$	$B_s \to D_s\pi$
data	60.0 ± 0.7	57.3 ± 1.0	49.1 ± 2.9	58.4 ± 0.5	57.2 ± 0.6	49.3 ± 2.3
nominal MC	55.2 ± 0.1	54.4 ± 0.1	49.5 ± 0.3	55.9 ± 0.1	56.6 ± 0.1	52.1 ± 0.3
fragmentation function	+2.5	+2.6	+2.3	+2.7	+3.0	+3.3
B^{**} rate	$^{+1.8}_{-0.5}$	$^{+2.0}_{-0.6}$	–	$^{+1.8}_{-0.5}$	$^{+2.0}_{-0.5}$	–
production mechanisms	$^{+0.7}_{-0.7}$	$^{+0.7}_{-0.7}$	$^{+0.6}_{-0.7}$	$^{+0.6}_{-0.5}$	$^{+0.7}_{-0.5}$	$^{+0.8}_{-0.7}$
multiple interactions	+0.1	+0.1	$^{+0.2}_{-0.1}$	+0.1	+0.1	± 0.1
varitation within data statistics	$^{+4.3}_{-0.2}$	$^{+3.4}_{-0.1}$	$^{+7.9}_{-0.3}$	$^{+3.4}_{-0.0}$	$^{+3.7}_{-0.0}$	$^{+2.0}_{-4.4}$
$\Sigma+$	+5.3	+4.8	+8.3	+4.8	+5.2	+3.9
$\Sigma-$	-0.9	-0.9	-0.8	-0.7	-0.7	-4.4

TABLE VIII: Systematic uncertainties on the tagging efficiency.

[%]	$B^+ \to J/\psi K^+$	$B^0 \to J/\psi K^*$	$B_s \to J/\psi\phi$	$B^+ \to D\pi$	$B^0 \to D\pi$	$B_s \to D_s\pi$
data	22.3 ± 1.9	10.7 ± 4.6	–	25.9 ± 1.4	13.3± 2.9	–
nominal MC	25.3 ± 0.2	14.9 ± 0.3	16.2 ± 0.8	25.7 ± 0.3	15.1 ± 0.4	19.0 ± 0.8
fragmentation function	+0.5	-0.1	+0.7	+0.7	$^{+0.1}_{-0.1}$	+1.7
B^{**} rate	$^{+2.2}_{-0.6}$	$^{+2.6}_{-0.7}$	–	$^{+2.3}_{-0.6}$	$^{+2.5}_{-0.6}$	–
production mechanisms	$^{+0.0}_{-0.2}$	$^{+0.3}_{-0.5}$	$^{+0.3}_{-0.7}$	$^{+0.2}_{-0.3}$	$^{+0.3}_{-0.5}$	$^{+0.3}_{-0.3}$
multiple interactions	$^{+0.0}_{-0.1}$	$^{+0.1}_{-0.1}$	$^{+0.0}_{-0.2}$	$^{+0.1}_{-0.0}$	$^{+0.0}_{-0.1}$	$^{+0.1}_{-0.0}$
kaon fraction	–	–	-2.4	–	–	-2.8
prompt kaon fraction	–	–	-2.0	–	–	-2.2
$V0$ content	–	–	$^{+0.1}_{-0.2}$	–	–	$^{+0.4}_{-0.3}$
variation within data statistics	$^{+1.1}_{-0.6}$	$^{+0.6}_{-0.7}$	$^{+0.5}_{-4.0}$	$^{+1.2}_{-0.4}$	$^{+0.4}_{-0.4}$	$^{+0.7}_{-2.4}$
$\Sigma+$	+2.5	+2.7	+0.9	+2.7	+2.5	+1.9
$\Sigma-$	-0.9	-1.1	-5.1	-0.8	-0.9	-4.4

TABLE IX: Systematic uncertainties on the average dilution of max p_L^{rel} algorithm.

Multiple Interactions
The rate of additional potential tagging tracks for high and low luminosity events has been measured on data and accordingly added to our Monte Carlo sample. The difference in tagger performance compared to a Monte Carlo with an average rate has been studied. As hard cuts on the impact parameter significance and the $\Delta z(B, track)$ are applied the effect of multiple interactions on the tagger performance is relatively small.

Tables VIII-XII summarize the results of the systematic uncertainties. The largest uncertainties for the B_s mesons come from the variation of the particle content around the B.

The distributions of track multiplicity with and without cut on the kaon probability and the particle ID distributions for all decay modes including the systematic variations are displayed in 19-22. The Monte Carlo distributions including the systematic variations enclose the data distributions.

Data Monte Carlo Agreement
Comparing the tagger dilution or dilution scale factors on data and Monte Carlo within their statistical and systematic uncertainties we see very good agreement. However this statement can not be made more precise than our uncertainties on the data and Monte Carlo sample. Therefore combined uncertainties from B^0 and B^+ modes have been added to the final result. This is done by computing the weighted mean of all four modes. All results are summarized in Table XIII.

The Data Monte Carlo agreement including statistical and systematical uncertainties for all algorithms studied are displayed in Figure 23. Additional to the 4 decay modes discussed in detail in previous sections, those plots show as well $B^+ \to D3\pi$ and $B^0 \to D3\pi$ data Monte Carlo comparisons. The reconstruction have been performed similar to [5]. The systematic uncertainties have been taken from the study of the according $D\pi$ modes. Due to trigger and reconstruction cuts those B candidates have in average a higher momentum thus a higher dilution. We see very good agreement in all modes and algorithms which makes us confident

[%]	$B^+ \to J/\Psi K$	$B^0 \to J/\Psi K^*$	$B_s \to J/\Psi\phi$	$B^+ \to D\pi$	$B^0 \to D\pi$	$B_s \to D_s\pi$
data	21.7 ± 1.9	10.7 ± 4.6	-	25.4 ± 1.4	14.2 ± 2.9	-
nominal MC	24.2 ± 0.3	12.7 ± 0.3	18.9 ± 0.8	24.5 ± 0.3	12.9 ± 0.4	21.8 ± 0.8
fragmentation function	$^{+0.4}_{-0.7}$	$^{+0.0}_{-0.2}$	$^{+0.9}_{-0.0}$	$^{+0.9}_{-0.2}$	$^{+0.0}_{-0.2}$	$^{+1.4}_{-0.0}$
PID simulation & resolution	$^{+0.1}_{-0.4}$	$^{+0.1}_{-0.1}$	$^{+0.0}_{-0.5}$	$^{+0.1}_{-0.4}$	$^{+0.1}_{-0.1}$	$^{+0.3}_{-0.2}$
B^{**} rate	$^{+2.1}_{-0.7}$	$^{+2.4}_{-0.7}$	-	$^{+2.1}_{-0.6}$	$^{+2.5}_{-0.6}$	-
production mechanisms	$^{+0.0}_{-0.3}$	$^{+0.2}_{-0.6}$	$^{+0.5}_{-0.6}$	$^{+0.1}_{-0.5}$	$^{+0.4}_{-0.5}$	$^{+0.0}_{-0.4}$
multiple interactions	$^{+0.1}_{-0.1}$	$^{+0.0}_{-0.1}$	$^{+0.0}_{-0.1}$	± 0.0	$^{+0.1}_{-0.0}$	$^{+0.1}_{-0.0}$
kaon fraction	-	-	-2.3	-	-	-2.6
prompt kaon fraction	-	-	-1.9	-	-	-3.8
resonance/V0 content	-	-	$^{+1.2}_{-0.7}$	-	-	$^{+1.2}_{-0.8}$
variation within data statistics	$^{+0.8}_{-1.1}$	$^{+0.2}_{-2.6}$	$^{+2.4}_{-3.6}$	$^{-0.7}_{+1.1}$	$^{+0.4}_{-0.7}$	$^{+2.0}_{-2.3}$
Σ^+	+2.3	+2.4	+2.9	+2.5	+2.6	+2.7
Σ^-	-1.6	-1.9	-4.8	-1.1	-1.1	-5.2

TABLE X: Systematic uncertainties on the average dilution of max $\log(LH(PID))$ algorithm.

[%]	$B^+ \to J/\psi K^+$	$B^0 \to J/\psi K^*$	$B_s \to J/\psi\phi$	$B^+ \to D\pi$	$B^0 \to D\pi$	$B_s \to D_s\pi$
data	91.8 ± 6.3	85.9 ± 29.1	–	103.6 ± 4.7	110.0 ± 16.0	–
nominal MC	100.3 ± 0.7	101.1 ± 1.8	99.7 ± 4.4	100.3 ± 0.9	98.0 ± 2.1	100.5 ± 3.3
fragmentation function	$^{+1.8}_{-0.5}$	$^{+0.2}_{-0.8}$	$^{+6.0}_{-0.0}$	$^{+2.2}_{-0.1}$	$^{+0.3}_{-0.6}$	$^{+6.3}_{-0.0}$
B^{**} rate	$^{+7,7}_{-1.8}$	$^{+17.4}_{-4.8}$	–	$^{10.2}_{-1.7}$	$^{+14.8}_{-4.3}$	–
production mechanisms	$^{+0.0}_{-0.9}$	$^{+0.4}_{-2.9}$	$^{+1.1}_{-2.5}$	$^{+0.6}_{-1.1}$	$^{+1.3}_{-2.9}$	$^{+0.0}_{-2.2}$
multiple interactions	$^{+0.0}_{-0.4}$	$^{+2.8}_{-0.0}$	$^{+0.0}_{-2.9}$	$^{+0.2}_{-0.1}$	$^{+0.1}_{-0.9}$	$^{+0.3}_{-0.0}$
kaon fraction	–	–	-13.9	–	–	-13.0
prompt kaon fraction	–	–	-11.6	–	–	-10.2
$V0$ content	–	–	$^{+5.0}_{-2.6}$	–	–	$^{+5.4}_{-1.1}$
variation within data statistics	$^{+1.0}_{-0.1}$	$^{+1.7}_{-2.0}$	$^{+1.7}_{-11.0}$	$^{+1.4}_{-0.0}$	$^{+1.0}_{-1.9}$	$^{+2.2}_{-5.9}$
$\Sigma+$	+8.0	+17.7	+8.0	+10.5	+14.9	+8.6
$\Sigma-$	-2.1	-6.0	-21.6	-2.0	-5.6	-17.7

TABLE XI: Systematic uncertainties on the dilution scale factor of max $p_{l,rel}$ algorithm.

about the predictions of the tagger performance for B_s.

[%]	$B^+ \to J/\psi K$	$B^0 \to J/\psi K^*$	$B_s \to J/\psi\phi$	$B^+ \to D\pi$	$B^0 \to D\pi$	$B_s \to D_s\pi$
data	87.6 ± 6.7	78.8 ± 25.1	–	95.1 ± 4.7	104.7 ± 14.4	–
nominal MC	100.0 ± 0.7	98.0 ± 1.7	98.8 ± 3.6	100.0 ± 0.9	98.5 ± 2.1	98.8 ± 2.5
fragmentation function	$^{+2.1}_{-0.1}$	$^{+0.3}_{-0.4}$	$^{+3.0}_{-0.0}$	$^{+2.5}_{-0.0}$	$^{+2.4}_{-0.6}$	$^{+4.4}_{-0.0}$
PID simulation & resolution	$^{+1.6}_{-3.1}$	$^{+1.8}_{-4.1}$	$^{+2.0}_{+6.1}$	$^{+1.7}_{-3.4}$	$^{+2.2}_{-3.1}$	$^{+3.6}_{-4.8}$
B^{**} rate	$^{+9.1}_{-2.5}$	$^{+12.1}_{-3.9}$	–	$^{+9.5}_{-2.4}$	$^{+14.6}_{-4.1}$	–
production mechanisms	$^{+0.0}_{-0.8}$	$^{+0.1}_{-2.0}$	$^{+2.0}_{-3.2}$	$^{+0.6}_{-1.2}$	$^{+0.3}_{-1.8}$	$^{+0.6}_{-1.5}$
multiple interactions	$^{+0.5}_{-0.6}$	$^{+0.1}_{-0.7}$	$^{+0.2}_{-0.8}$	$^{+0.2}_{-0.1}$	$^{+0.1}_{-0.5}$	$^{+0.2}_{-0.2}$
kaon fraction	–	–	-9.2	–	–	-5.8
prompt kaon fraction	–	–	-8.8	–	–	-6.4
resonance/$V0$ content	–	–	$^{+5.8}_{-6.1}$	–	–	$^{+4.0}_{-4.1}$
variation within data statistics	$^{+2.3}_{-0.6}$	$^{+1.4}_{-2.0}$	$^{+3.1}_{-11.4}$	$^{+2.7}_{-0.0}$	$^{+2.4}_{-2.2}$	$^{+1.6}_{-4.3}$
$\Sigma+$	+9.8	+12.3	+7.7	+10.0	+15.2	+7.1
$\Sigma-$	-4.1	-4.8	-19.4	-4.3	-5.9	-11.8

TABLE XII: Systematic uncertainties on the dilution scale factor of max $\log(LH(PID))$ algorithm.

algorithm [%]	value	stat MC	sys MC	data/MC agreement	$\sum$
average dil, max. p_L^{rel}	19.0	$\pm$ 0.8	${}^{+1.9}_{-4.4}$	$\pm$ 2.1	${}^{+2.9}_{-4.9}$
average dil, max. PID	21.8	$\pm$ 0.8	${}^{+2.7}_{-5.2}$	$\pm$ 1.6	${}^{+3.2}_{-5.5}$
predicted dil, max. p_L^{rel}	100.5	$\pm$ 3.3	${}^{+8.6}_{-17.7}$	$\pm$ 5.5	${}^{+10.7}_{-18.8}$
predicted dil, max. PID	98.8	$\pm$ 2.5	${}^{+7.1}_{-11.8}$	$\pm$ 7.6	${}^{+10.7}_{-14.3}$

TABLE XIII: Summary of tagging performance and according uncertainties for $B_s \to D_s\pi$.

V. CONCLUSION

We evaluated based on a Monte Carlo sample the performance of different SS(K)T algorithms on B^+, B^0 and B_s decay modes. All tagging algorithms show very good data Monte Carlo agreement for the B^0 and B^+ modes. A kaon ID based algorithm using with event-by-event predicted dilutions turned out to perform best for tagging B_s mesons, further optimizations are possible. We evaluated in detail systematic uncertainties for potential discrepancies between data and Monte Carlo. Our final result is a dilution scale factor of

$$S_D = 98.8^{+10.7}_{-14.3}\ \%,$$

which results in an effective tagging dilution and tagging performance of:

$$S_D\sqrt{< D^2 >} = 28.3^{+3.2}_{-4.2}\ \%$$
$$\epsilon S_D^2 < D^2 >= 4.0^{+0.9}_{-1.2}\ \%$$

where the efficiency ϵ and the squared expectation value of the dilution $< D^2 >$ are taken from the $B_s \to D_s\pi$ data sample.

[1] CDF Collaboration,
Updated Measurement of Δm_d and Calibration of Flavor Tagging in Fully Reconstructed Decays,
CDF Public Note 7920

[2] CDF Collaboration,
B_d^0 Mixing and Taggers Performance in Semileptonic B Decays in the Two-Track Trigger Sample,
CDF Public Note 7910

[3] CDF Collaboration,
Scale Factors for Proper Time Uncertainties with Event-by-Event Primary Vertex Reconstruction,
CDF Public Note 7944

[4] CDF Collaboration,
Study of $B_s^0 \to \ell^+ D_s^- X$ Oscillations in the Two-Track Trigger Sample
CDF Public Note 7907

[5] CDF Collaboration,
Updated Study of B_s^0 Oscillations in $B_s^0 \to D_s^-(3)\pi$,
CDF Public Note 7941

[6] T. Sjörstrand, et al,
Comp. Phys. Commun. **135**, 238 (2001);

[7] E. Ben-Haim, P. Bambade, P. Roudeau, A. Savoy-Navarro and A. Stocchi,
Extraction of the x-dependence of the non-perturbative QCD b-quark fragmentation distribution component,
Phys. Lett. B **580**, 108 (2004) [arXiv:hep-ph/0302157].

[8] M. Gronau, A. Nippe, J. Rosner,
Phys. Rev. D **47**, 1988 (1993);
M. Gronau, J. Rosner,
Phys. Rev. D **49** 254 (1994)

[9] among many others:
DELPHI Collaboration, *A Study of Excited b-Hadron Sates with the DELPHI Detector at LEP*, `http://delphiwww.cern.ch/pubxx/conferences/summer05/paper_lp56.ps.gz`,
ALEPH Collaboration,
Production of excited beauty states in Z decays
Z. Phys. C 69, 393 (1996)

[10] CDF Collaboration,
Observation of Orbitally Excited B Mesons in $p\bar{p}$ Collisions at $\sqrt{s} = 1.8 TeV$,
Phys. Rev. D 64, 072002 (2001)

[11] CDF Collaboration,
Study of Charged Particles Species Produced in Association with $\bar{B}^0$, B^- and B_s Mesons in $p\bar{p}$ Collisions at $\sqrt{s} = 1.96\ TeV$.
CDF Public Note 8137

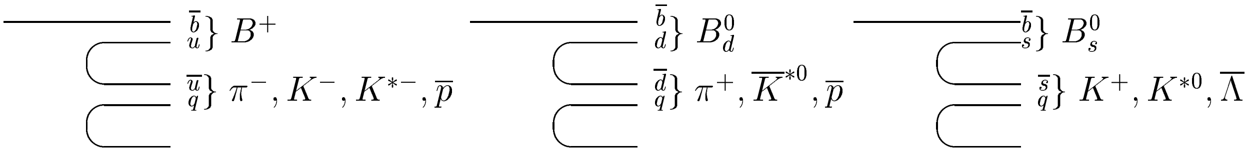

FIG. 1: Charge correlation of B mesons with fragmentation tracks.

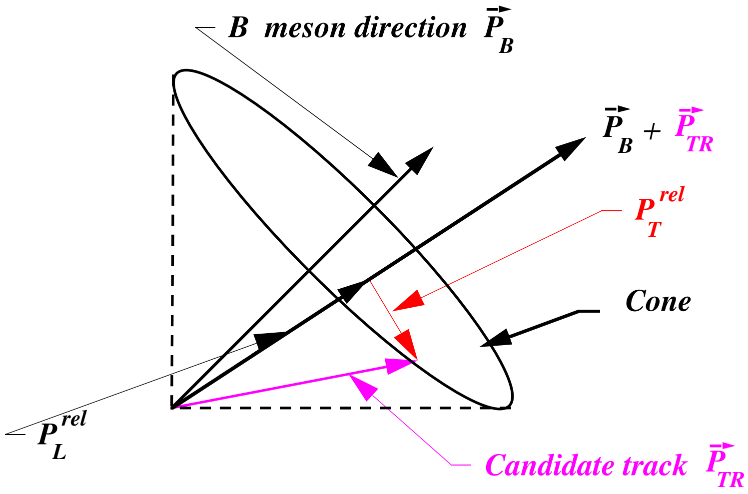

FIG. 2: Illustration of the construction of the quantity p_T^{rel}.

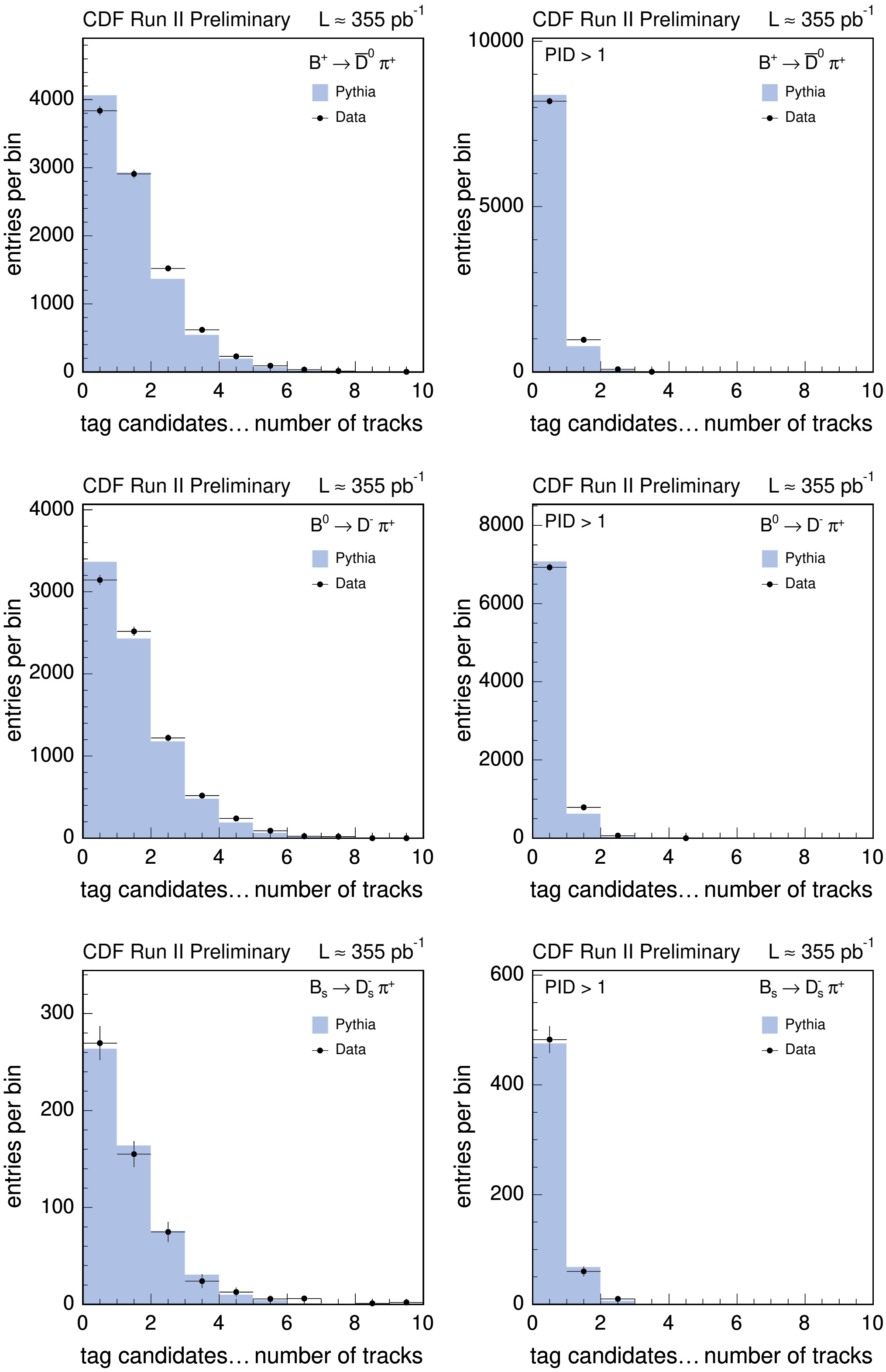

FIG. 3: Data and Monte Carlo comparisons of the tagging tracks multiplicity. On the right column we request $\log(PID) > 1$.

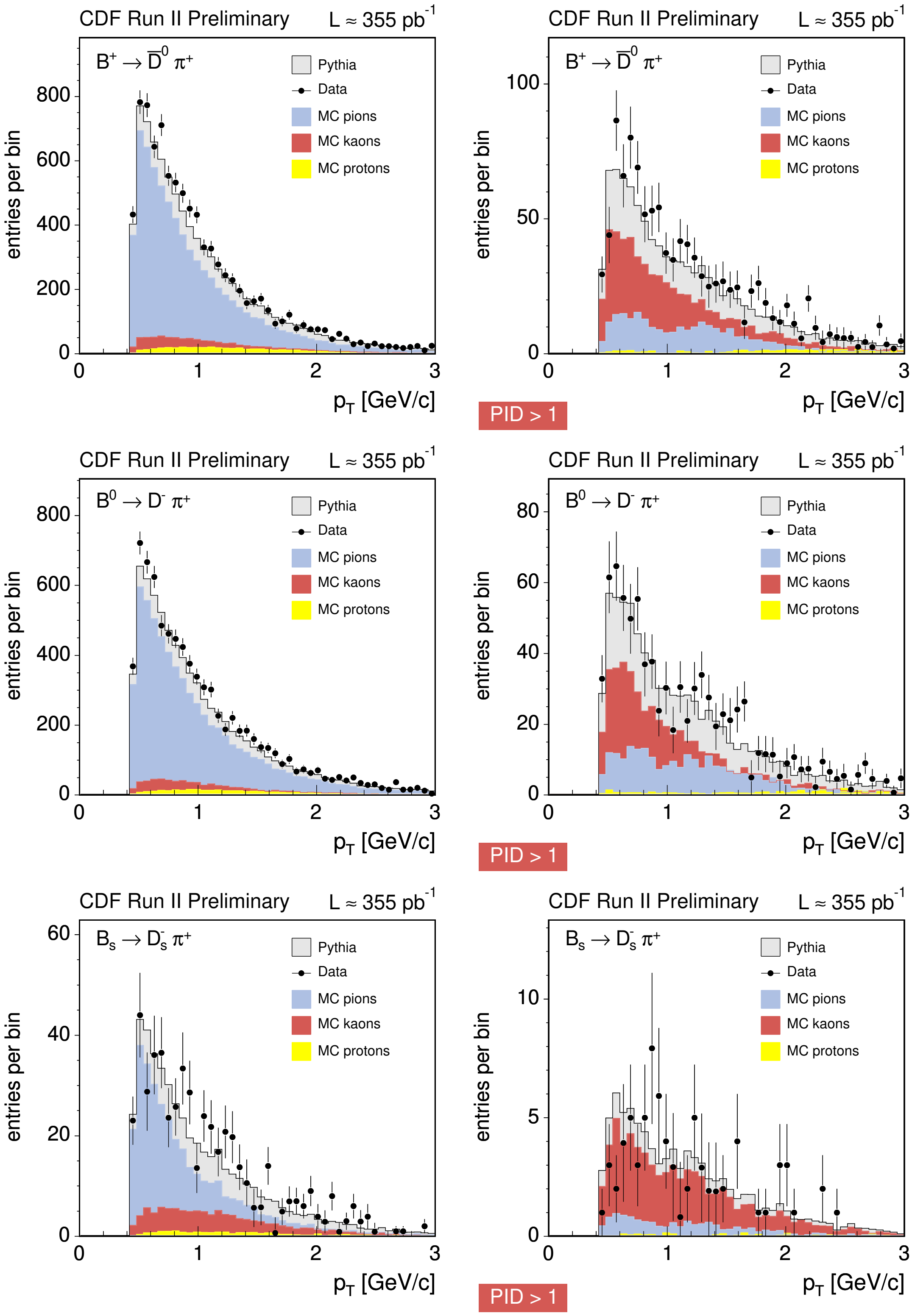

FIG. 4: Tagging candidates p_T comparisons between data (black dots) and MC (solid histograms). On the right column we request $\log(PID) > 1$.

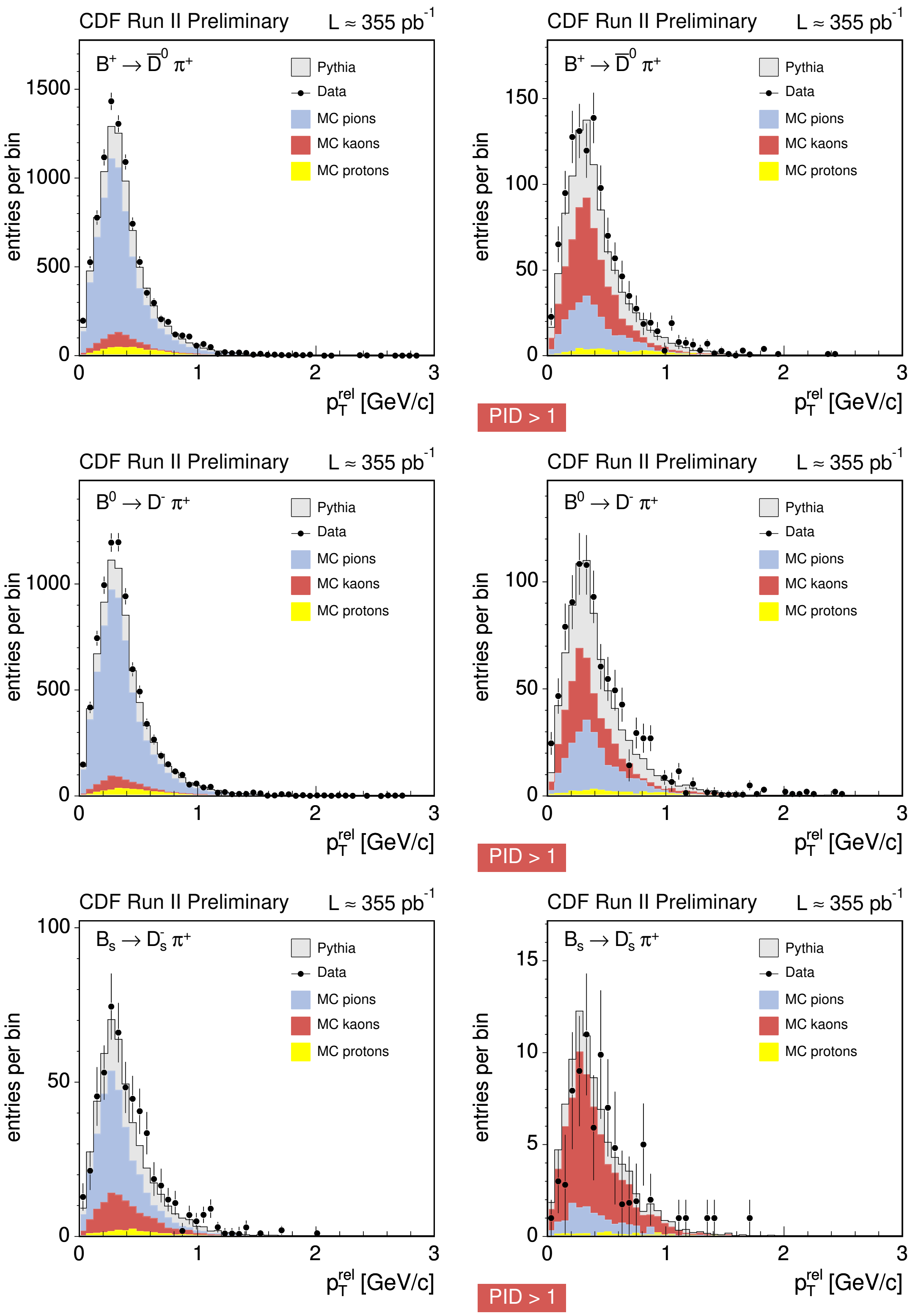

FIG. 5: Tagging candidates p_T^{rel} comparisons between data (black dots) and MC (solid histograms). On the right column we request $\log(PID) > 1$.

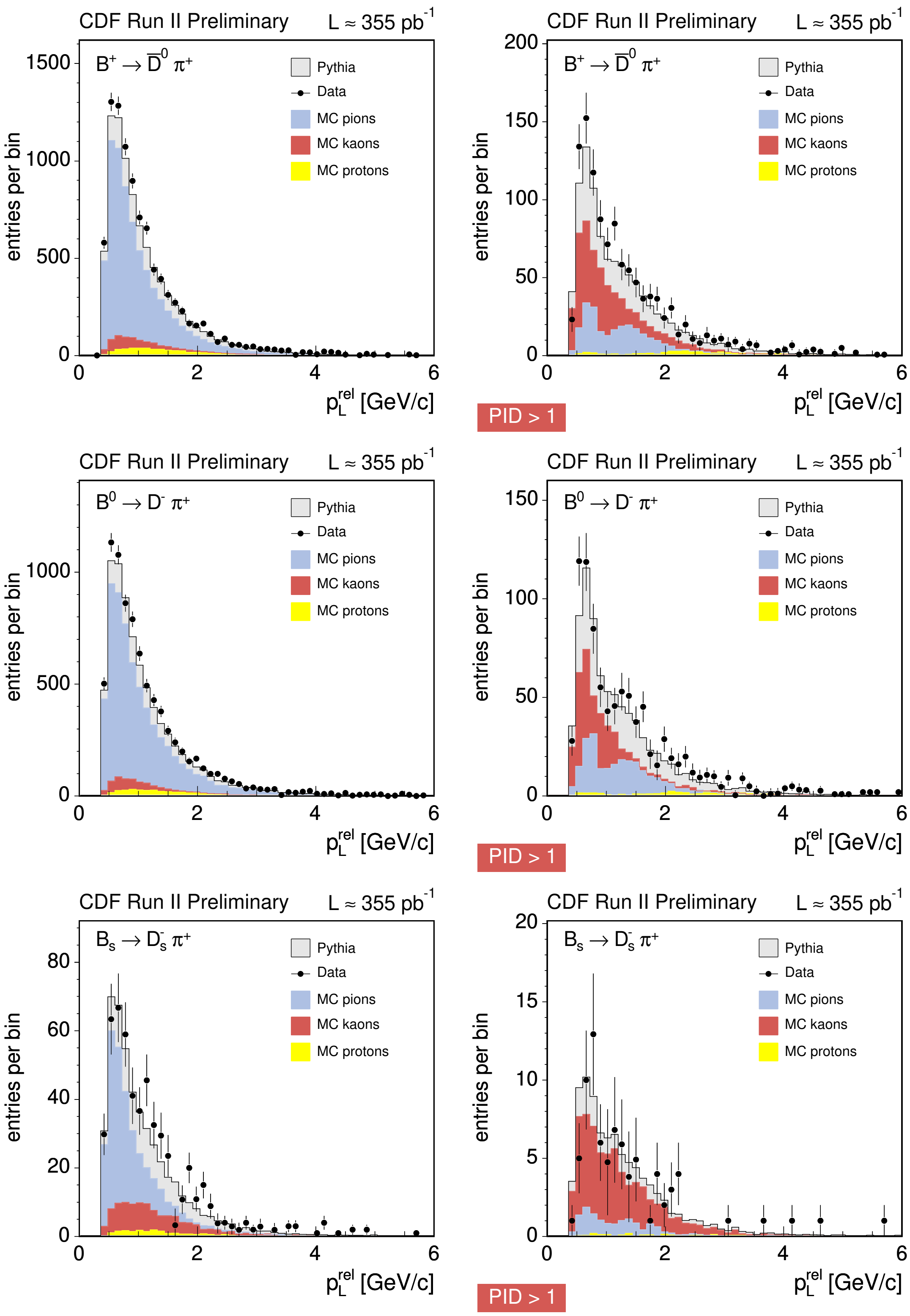

FIG. 6: Tagging candidates p_L^{rel} comparisons between data (black dots) and MC (solid histograms). On the right column we request $\log(PID) > 1$.

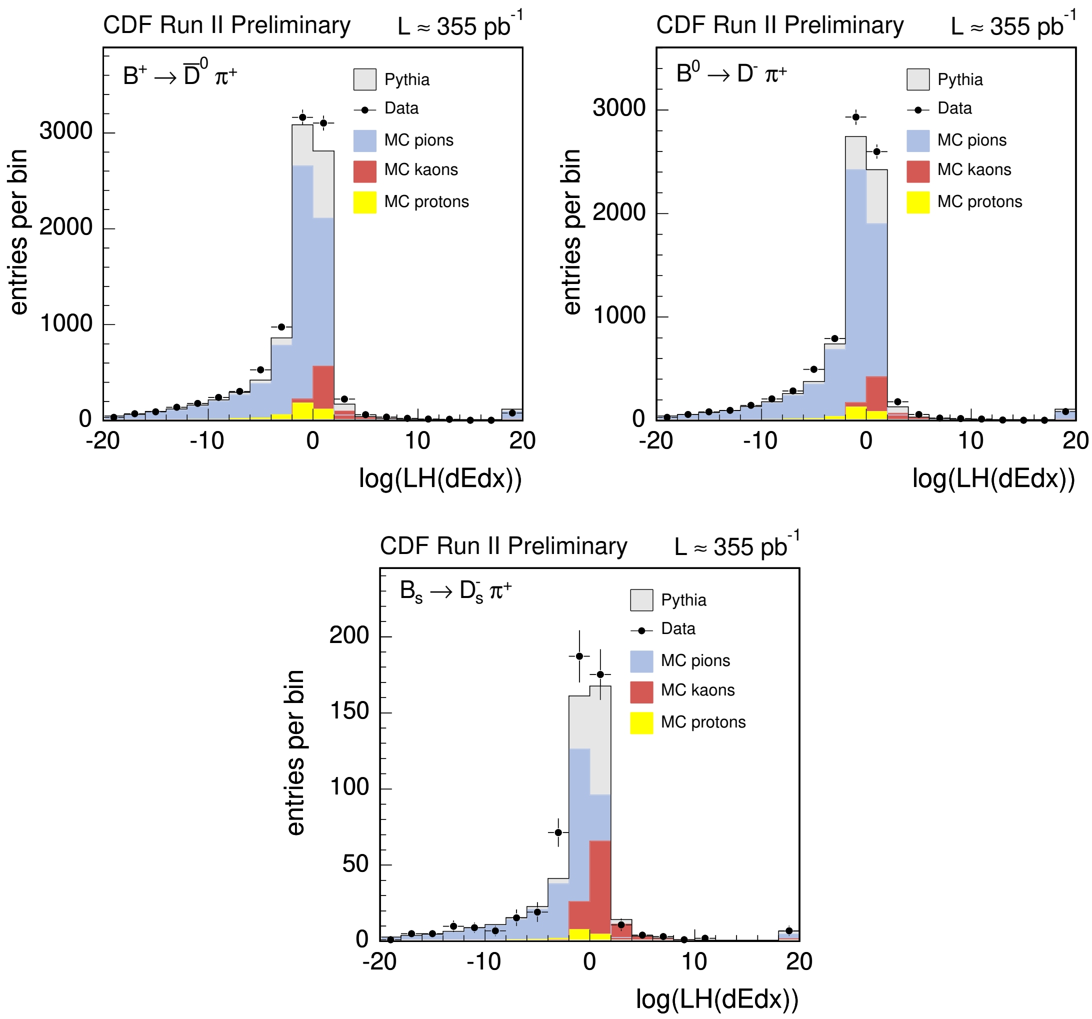

FIG. 7: Comparison of the $\log(LH(TOF))$ distributions between data (black dots) and Monte Carlo (light grey histogram). Bin "19" corresponds to no Tof information available for those tracks.

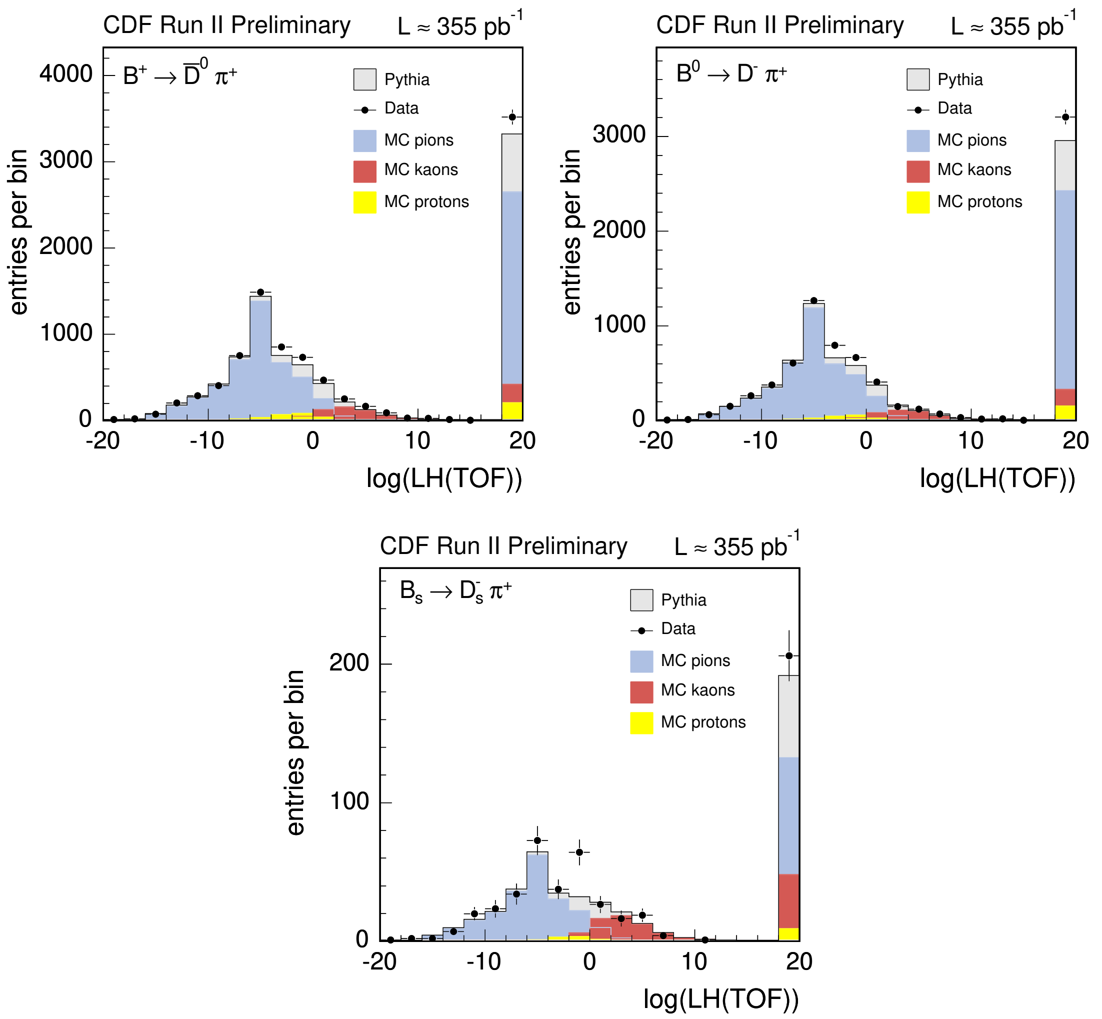

FIG. 8: Comparison of the $\log(LH(dE/dx))$ distributions between data (black dots) and Monte Carlo (light grey histogram). Bin "19" corresponds to no Tof information available for those tracks.

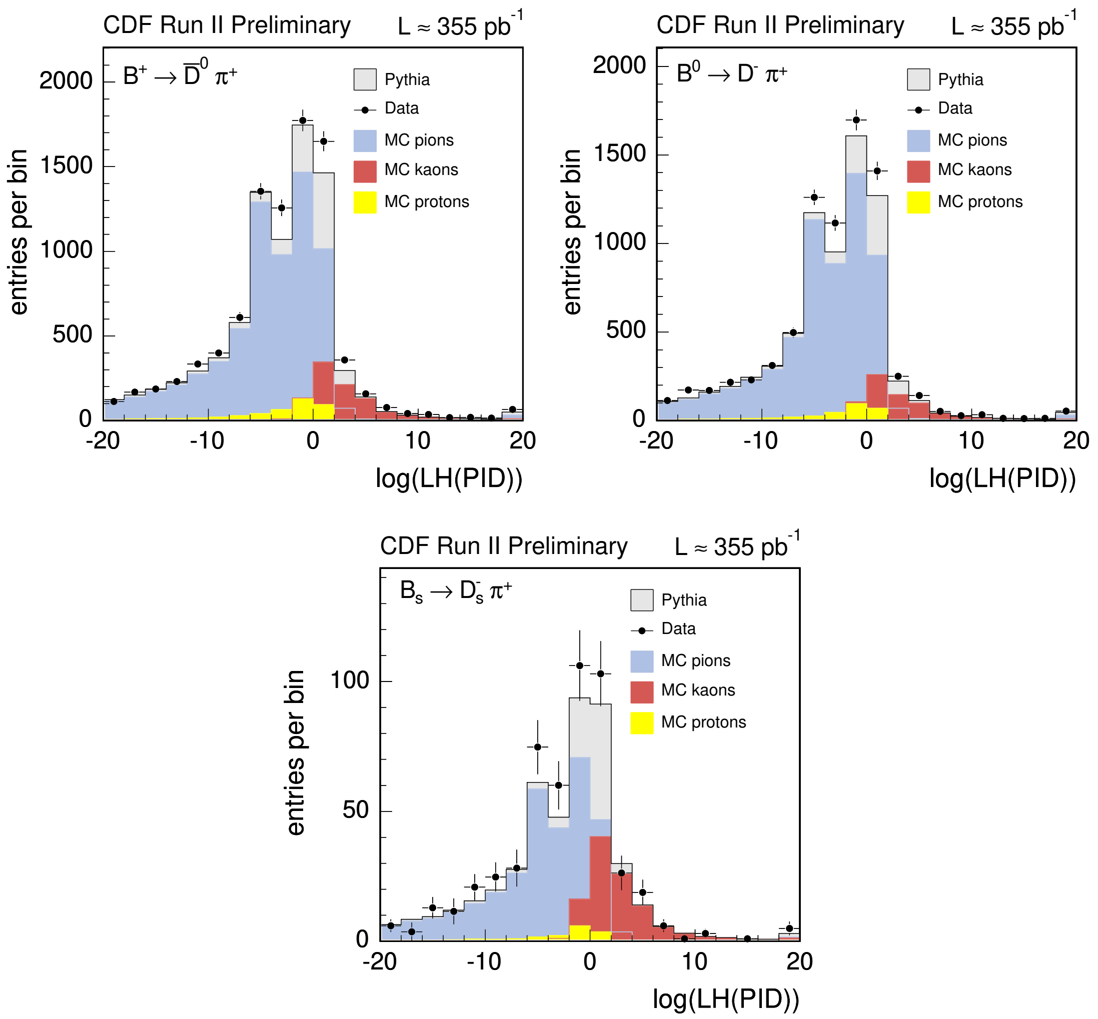

FIG. 9: Comparison of the $\log(LH(PID))$ distributions between data (black dots) and Monte Carlo (light grey histogram). Bin "19" corresponds to no particle ID information available for those tracks.

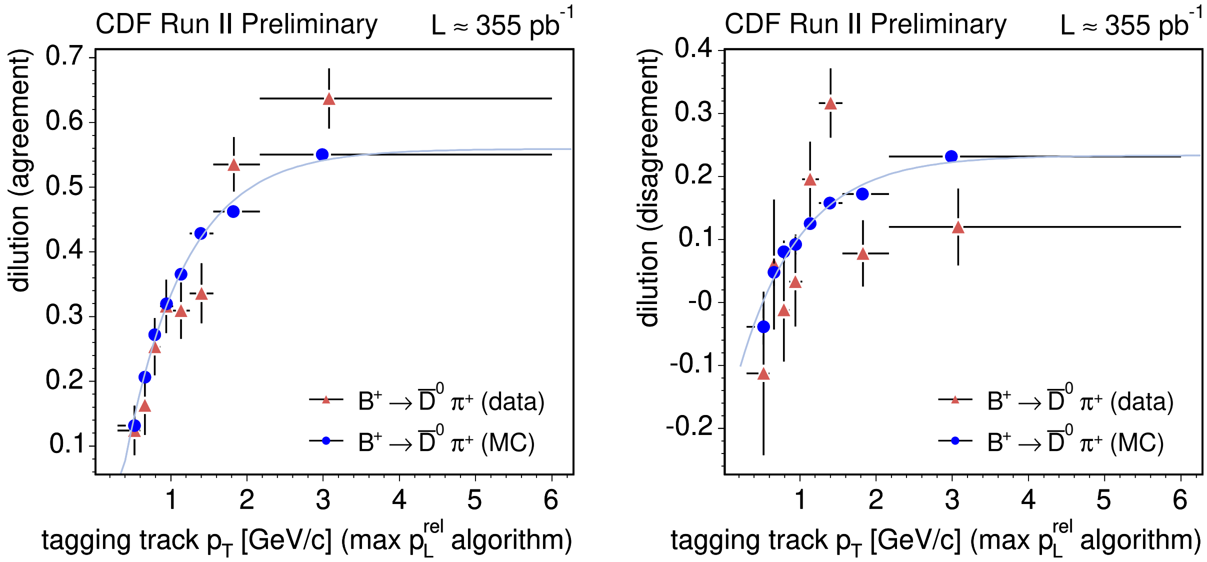

FIG. 10: Dilution of max $p_{l,rel}$ algorithm as a function of the p_T of the tagging track for cases of agreeing tagging candidate charges and disagreeing ones for $B^+ \to \bar{D}^0\pi^+$. Light blue line corresponds to the event-by-event predicted dilution function which has been derived from Monte Carlo.

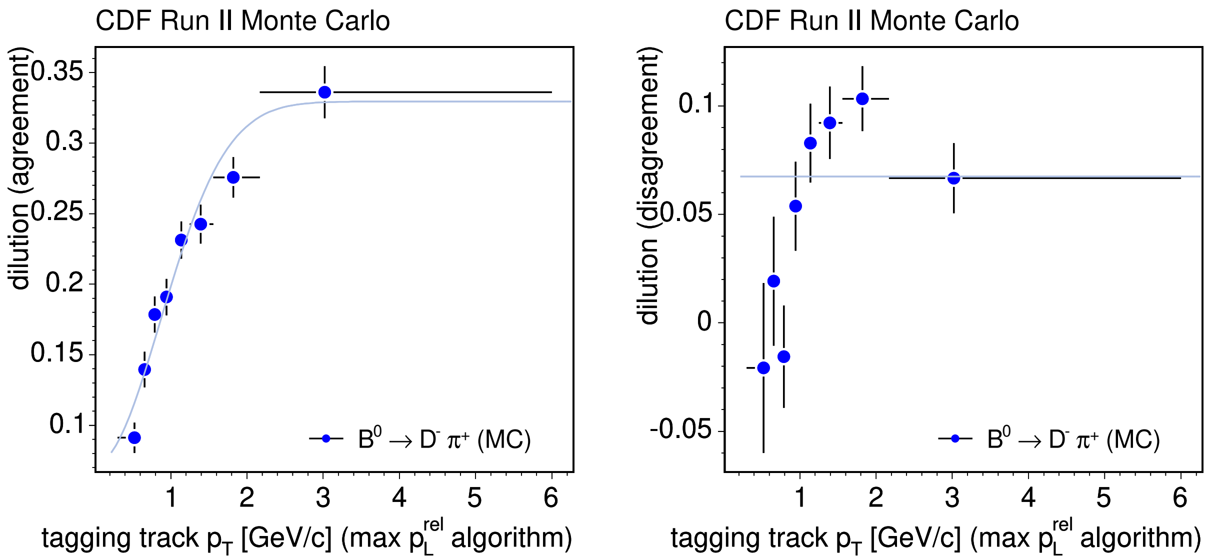

FIG. 11: Dilution of max $p_{l,rel}$ algorithm as a function of the p_T of the tagging track for cases of agreeing tagging candidate charges and disagreeing ones for $B^0 \to D^-\pi^+$. Light blue line corresponds to the event-by-event predicted dilution function, which has been derived from Monte Carlo.

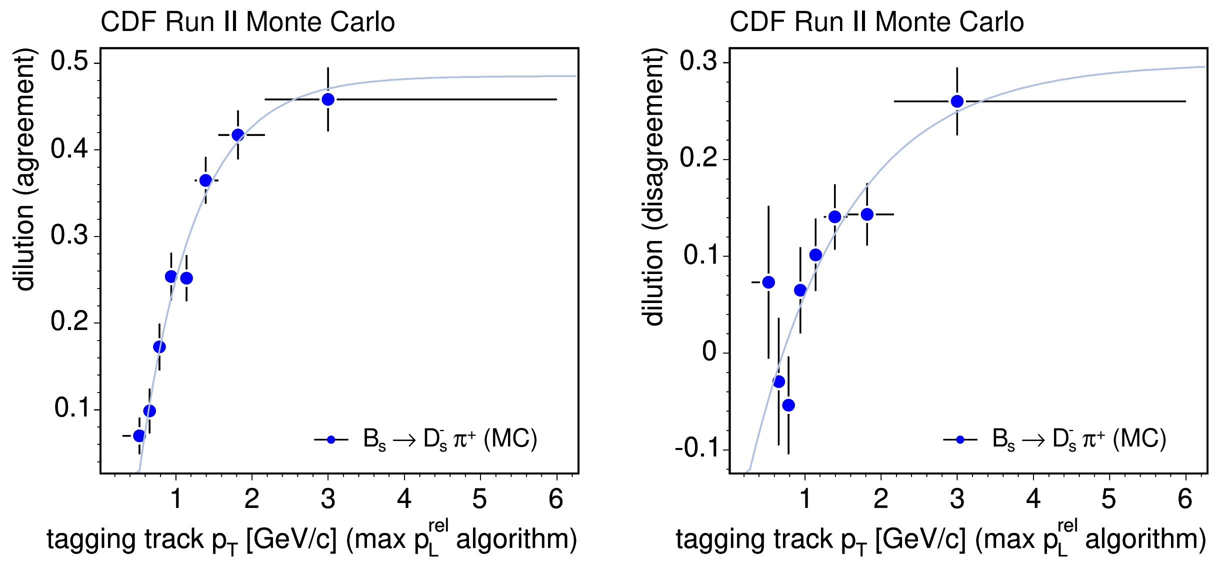

FIG. 12: Dilution of max $p_{l,rel}$ algorithm as a function of the p_T of the tagging track for cases of agreeing tagging candidate charges and disagreeing ones for $B_s \to D_s^- \pi^+$ decay. Light blue line corresponds to the event-by-event predicted dilution function, which has been derived from Monte Carlo.

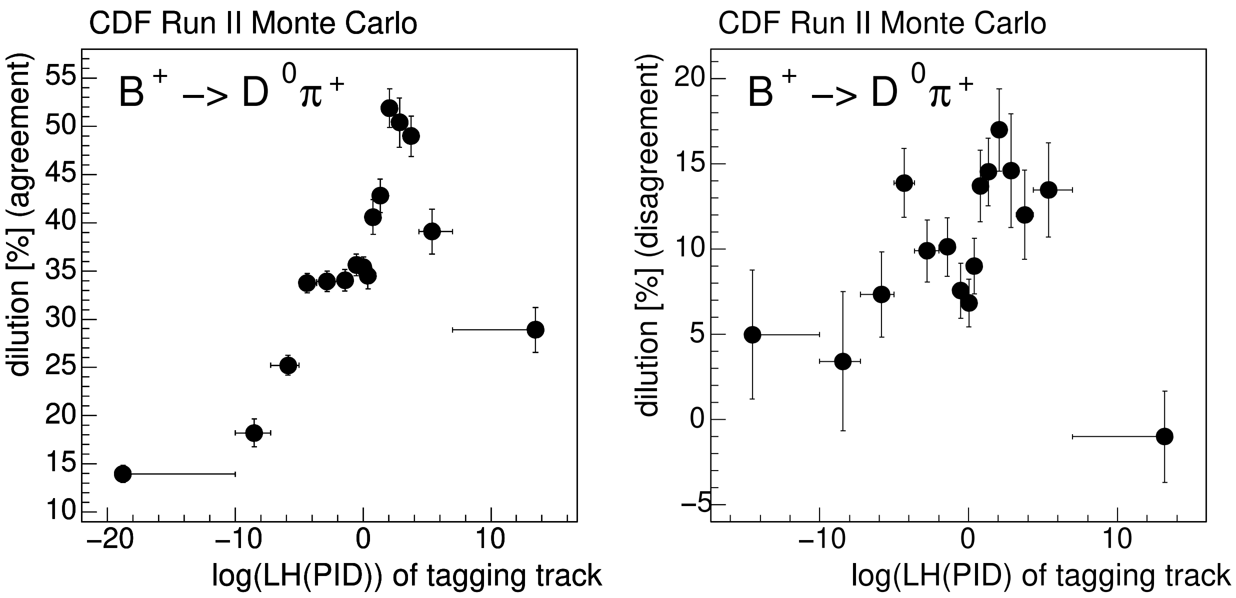

FIG. 13: Dilution of max $\log(LH(PID))$ algorithm as a function of the $\log(LH(PID))$ of the tagging track for cases of agreeing tagging candidate charges and disagreeing ones $B^+ \to D\pi$. As the shape of the dilution dependency on $\log(LH(PID))$ is hard to parameterized a bin-per-bin parameterization has been chosen.

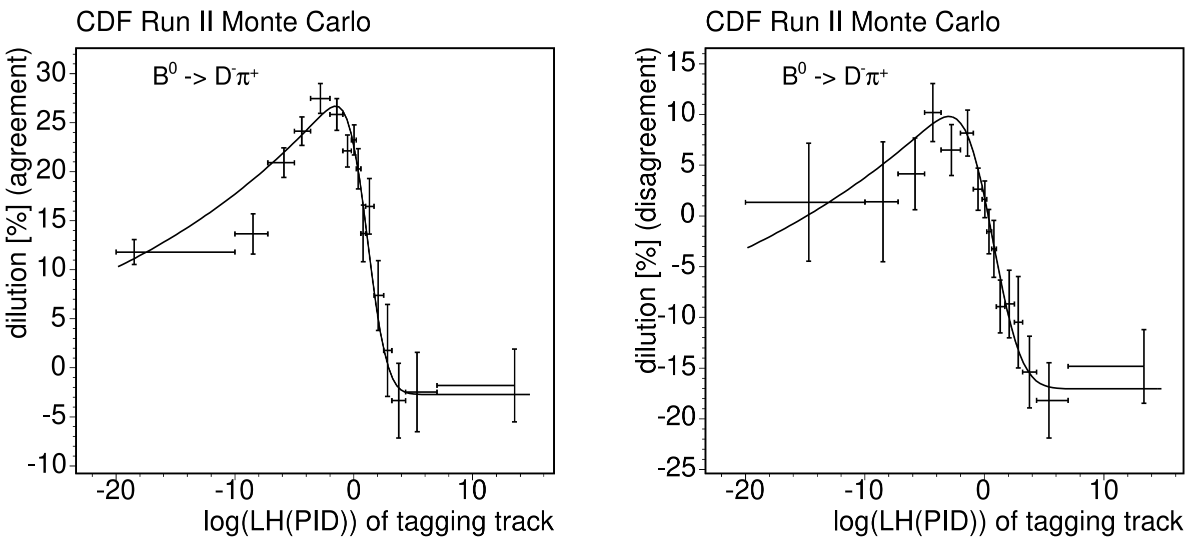

FIG. 14: Dilution of max $\log(LH(PID))$ algorithm as a function of $\log(LH(PID))$ of the tagging track for cases of agreeing tagging candidate charges and disagreeing ones for $B^0 \to D^-\pi^+$. Black line correspond to the event-by-event predicted dilution function, which has been derived from Monte Carlo.

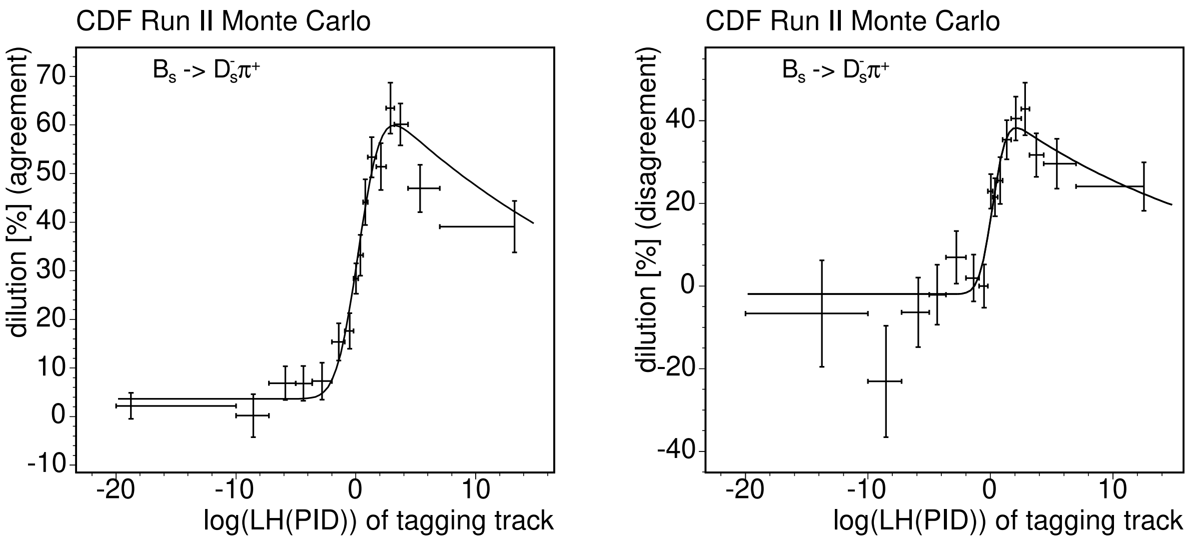

FIG. 15: Dilution of max $\log(LH(PID)$ algorithm as a function of the $\log(LH(PID))$ of the tagging track for cases of agreeing tagging candidate charges and disagreeing ones for $B_s \to D_s^-\pi^+$. Black line correspond to the event-by-event predicted dilution function, which has been derived from Monte Carlo.

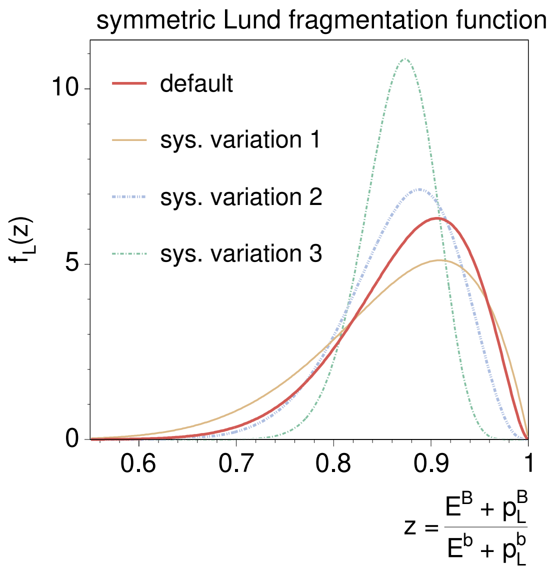

FIG. 16: Lund fragmentation function $f_L(z)$ where z is the ratio of the sum of energy and longitudinal momentum of the B meson and the b string.

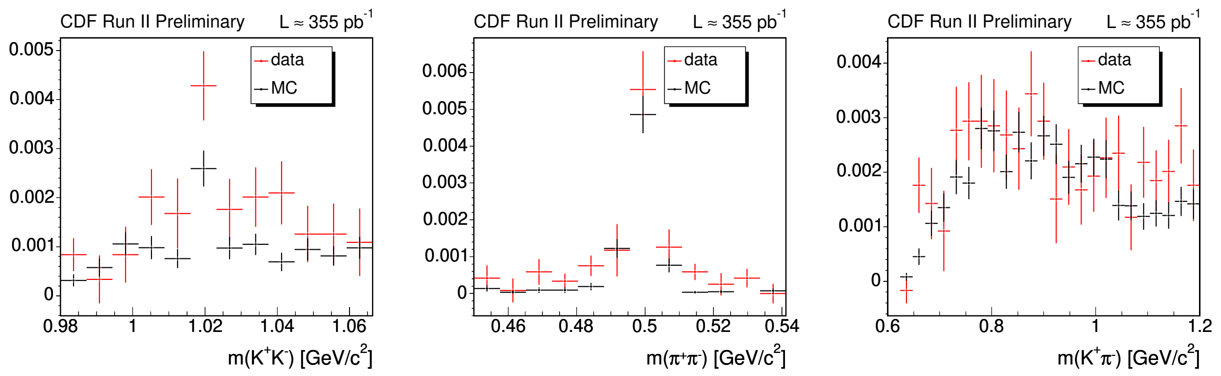

FIG. 17: Reconstructed ϕ, K_s and K^* candidates, where at least one leg is required to be within the code of $\Delta R = 0.7$ around the B_s direction. Black dots correspond to $B_s \to D\pi$ Monte Carlo, red dots to $B_s \to \ell D_s(\phi\pi)$ on data. Plots are normalized to the number of reconstructed B_s candidates.

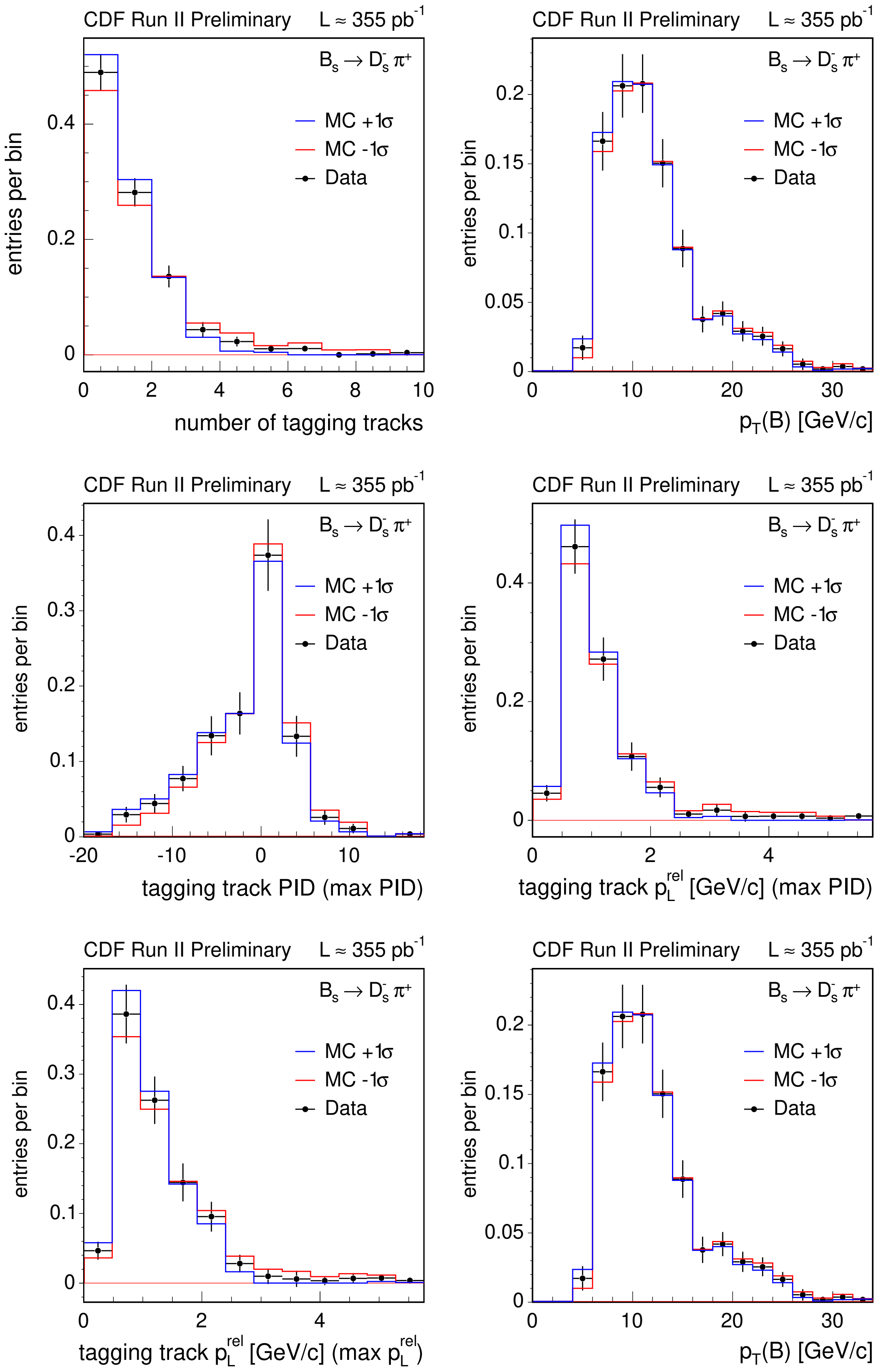

FIG. 18: Variation of data quantities (black points) within there uncertainties to lower mean value (blue) and to higher mean values (red) for $B_s \to D_s\pi$ modes.

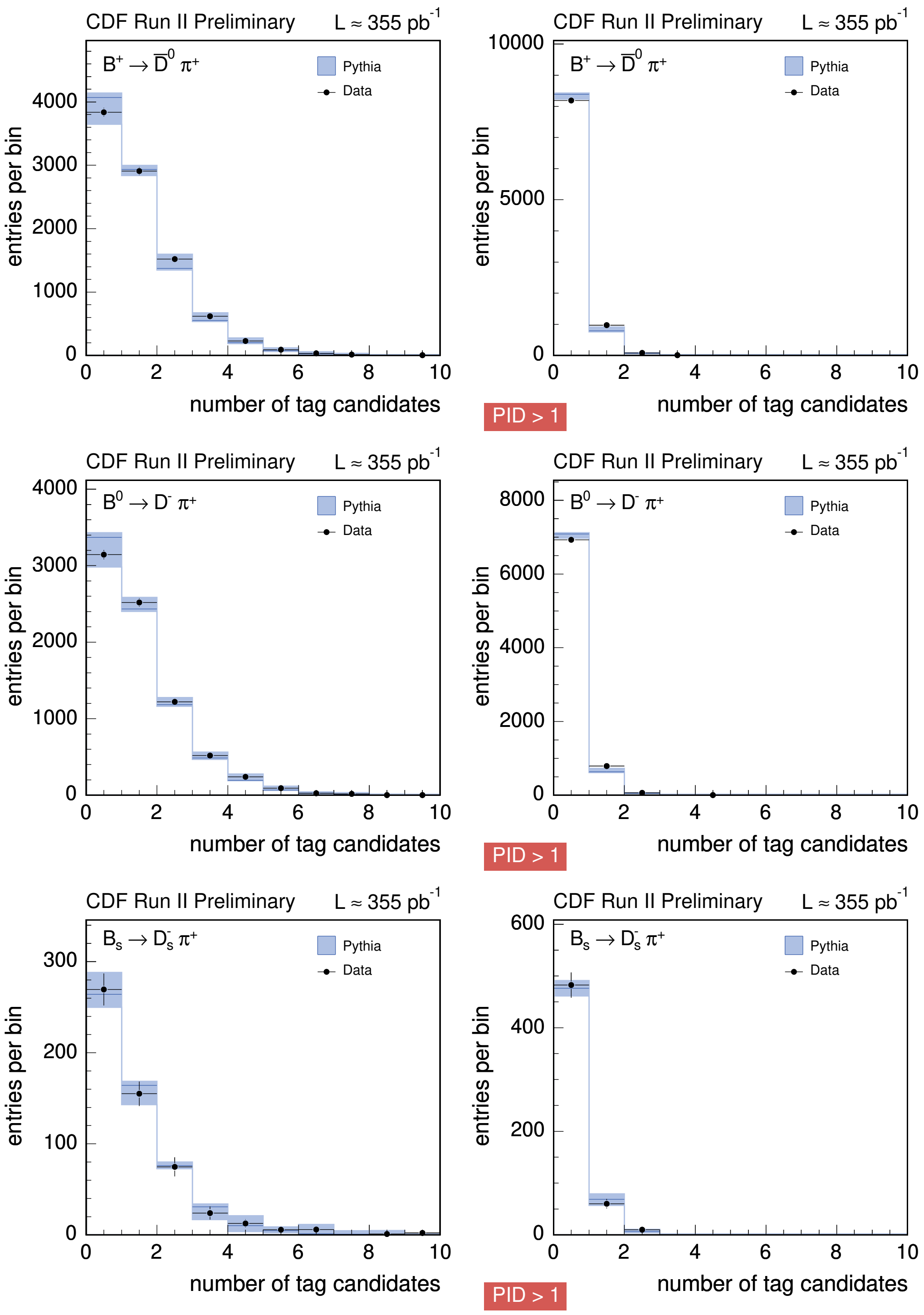

FIG. 19: Data and Monte Carlo comparisons of the tagging tracks multiplicity, for the $D\pi$ decay modes. On the right column we request $\log(LH(PID)) > 1$. The blue band corresponds to systematic variations applied to the Monte Carlo sample.

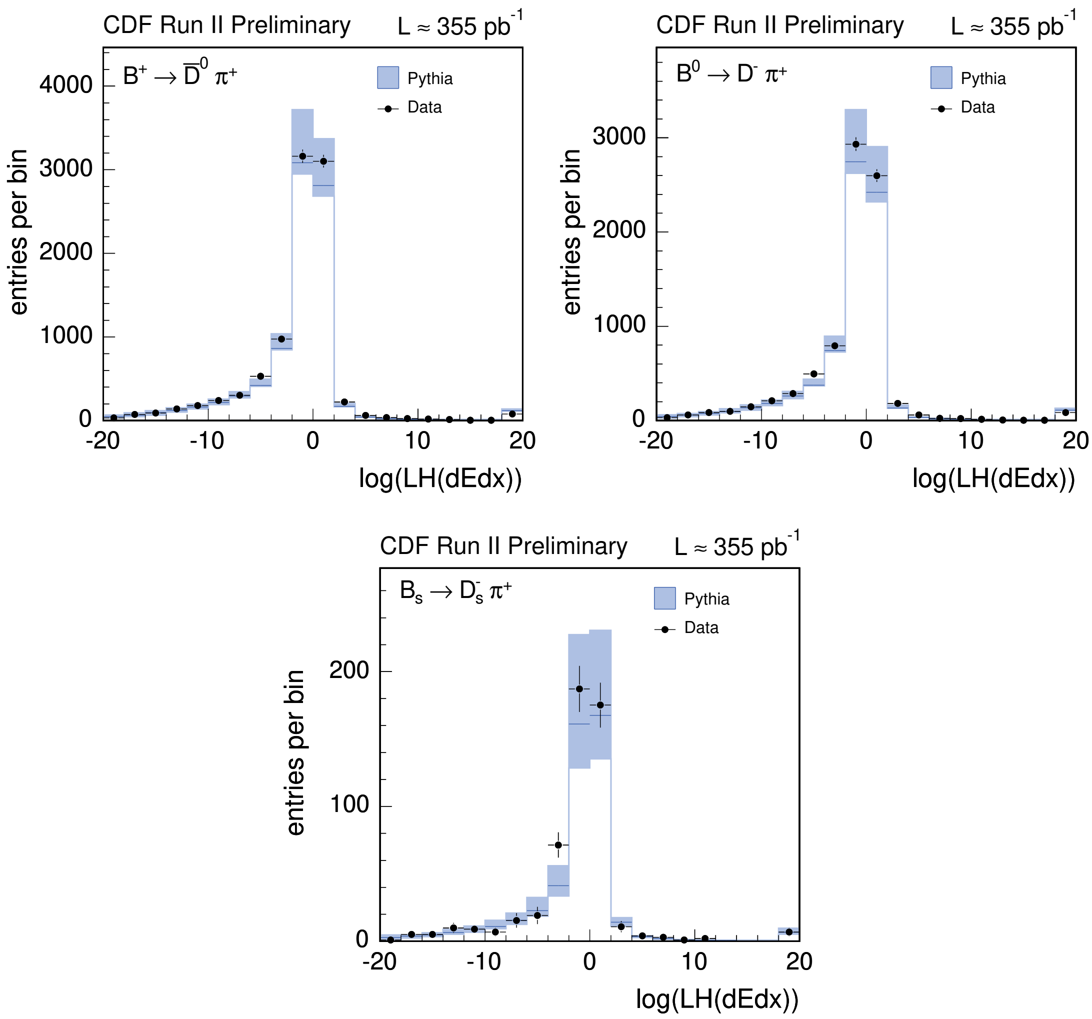

FIG. 20: Comparison of the $\log(LH(dE/dx))$ distributions between data (black dots) and Monte Carlo (light blue histogram). Bin "19" corresponds to no dE/dx information available for those tracks. The blue band corresponds to systematic variations applied to the Monte Carlo sample.

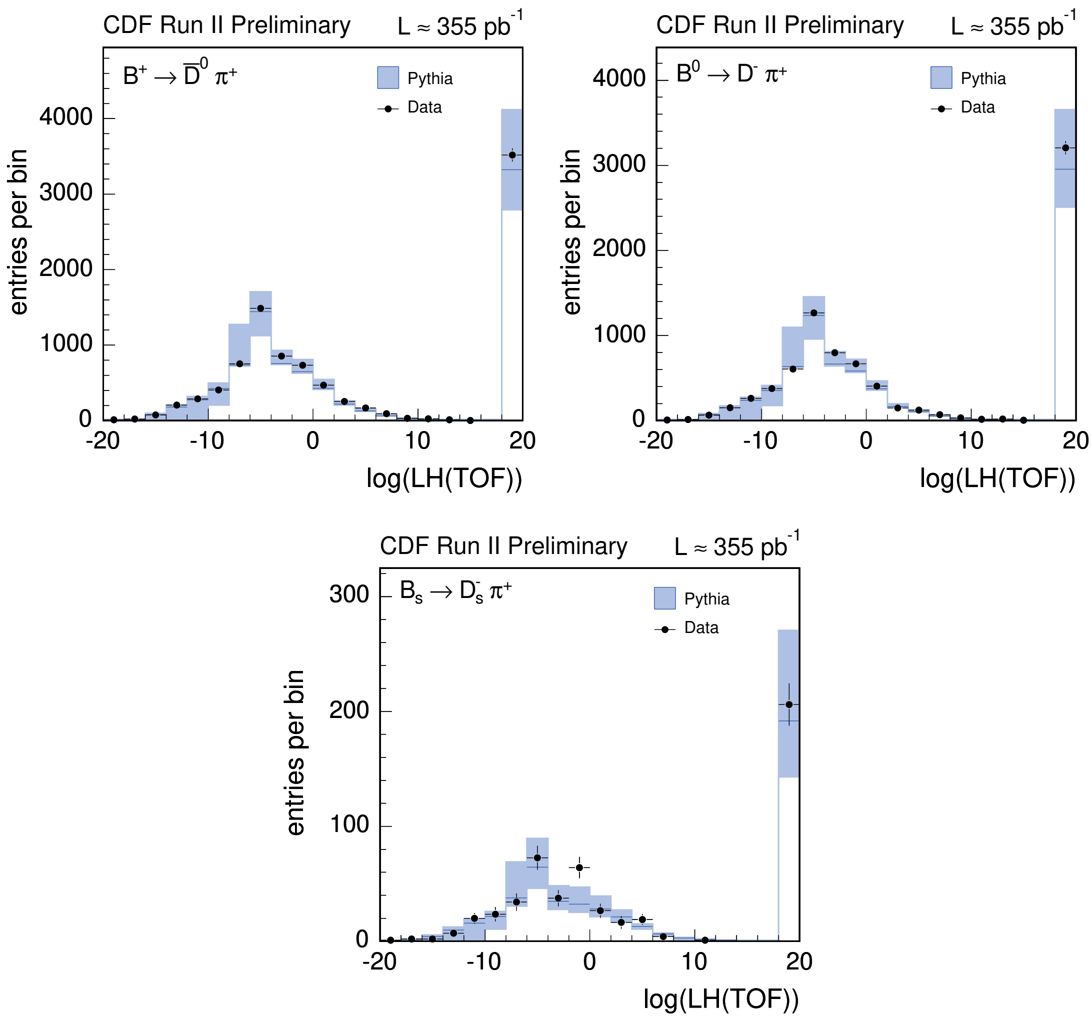

FIG. 21: Comparison of the $\log(LH(Tof))$ distributions between data (black dots) and Monte Carlo (light blue histogram). Bin "19" corresponds to no Tof information available for those tracks. The blue band corresponds to systematic variations applied to the Monte Carlo sample.

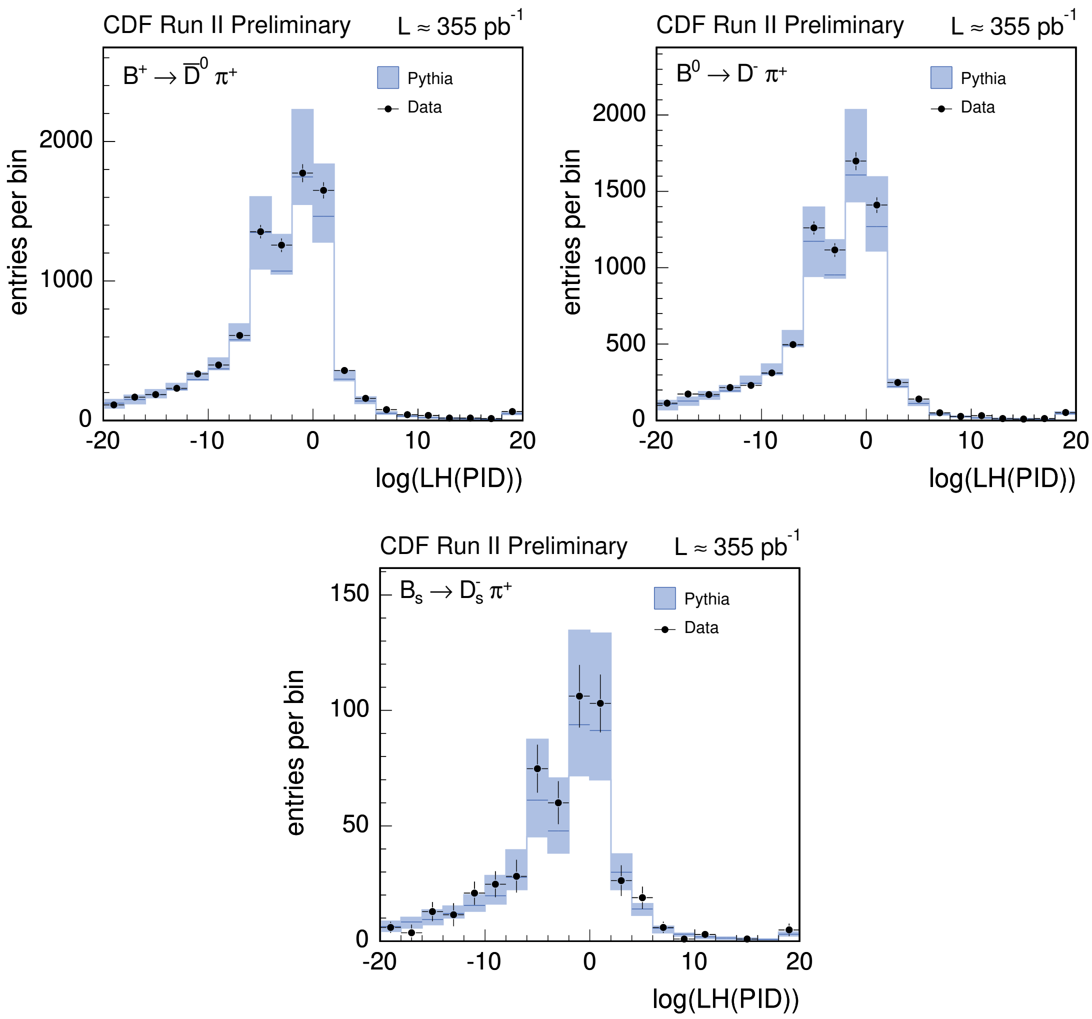

FIG. 22: Comparison of the $\log(LH(PID))$ distributions between data (black dots) and Monte Carlo (light blue histogram). Bin "19" corresponds to no particle ID information available for those tracks. The blue band corresponds to systematic variations applied to the Monte Carlo sample.

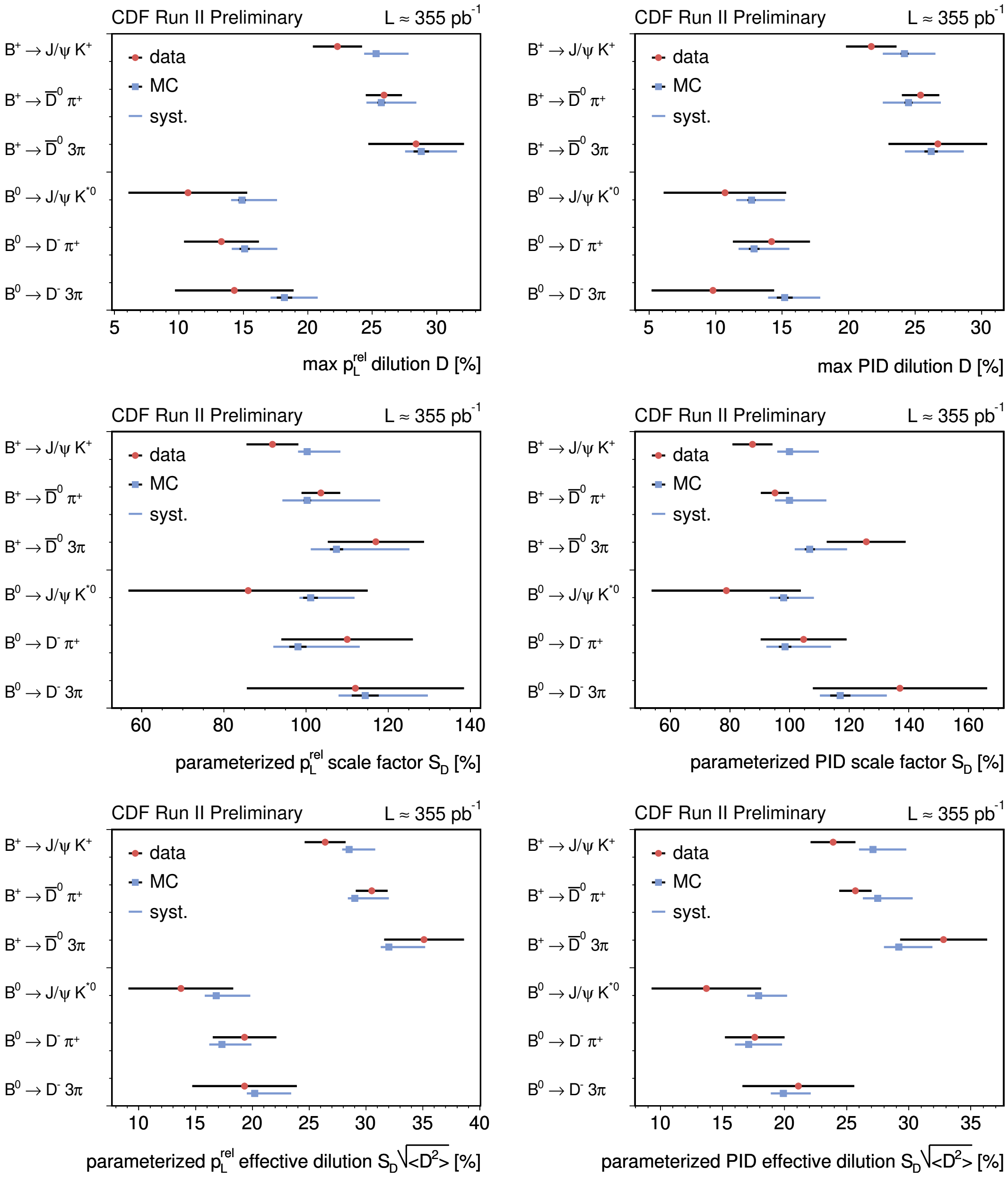

FIG. 23: Comparison of tagger performance of different algorithms for data and Monte Carlo for 3 different B^0 and B^+ modes.